European Journal of Pharmaceutics and Biopharmaceutics 158 (2021) 211–221

Contents lists available at ScienceDirect

European Journal of Pharmaceutics and Biopharmaceutics

journal homepage: www.elsevier.com/locate/ejpb

Lipid-encapsulated upconversion nanoparticle for near-infrared light-mediated carbon monoxide release for cancer gas therapy

Yaw Opoku-Damoah [a], Run Zhang [a,*], Hang T. Ta [a,b,c], D. Amilan Jose [d], Rahul Sakla [d], Zhi Ping Xu [a,*]

[a] Australian Institute for Bioengineering and Nanotechnology, The University of Queensland, Brisbane, QLD 4072, Australia
[b] School of Environment and Science, Griffith University, Brisbane, QLD 4111, Australia
[c] Queensland Micro and Nanotechnology Centre, Griffith University, Brisbane, QLD 4111, Australia
[d] Department of Chemistry, National Institute of Technology (NIT) at Kurukshetra, Kurukshetra 136119, Haryana, India

ARTICLE INFO

Keywords:
Cancer gas therapy
Carbon monoxide-releasing molecule
Upconversion nanoparticles
Targeted delivery
NIR-triggered CO-prodrug delivery system

ABSTRACT

Cancer gas therapy is just in an early stage of research and development. Several important gasotransmitters have proven their therapeutic potentials, but handling, delivery and controlled release of these gases remain very challenging for therapeutic purposes. This research develops a versatile nanosystem that is capable of delivering carbon monoxide (CO) gasotransmitter in the form of photo-responsive carbon monoxide-releasing molecule (CORM) for targeted cancer therapy. The core-shell upconversion nanoparticles (UCNPs) were designed to transfer bio-friendly low energy near infrared (NIR) light to ultraviolet (UV) light and trigger CO release from the loaded CORM. The synthesized delivery system demonstrated its ability to mediate the sustained release of CO upon 808 or 980 nm NIR light excitation. The optimized nanoformulation was efficiently taken up by HCT116 cancer cells and showed dose-dependent cytotoxicity to HCT116 and other cancer cells. Intracellular CO release and subsequent therapeutic action involving ROS production were found to significantly contribute to cell apoptosis. Therefore, the current research demonstrates the potency and efficiency of an NIR-mediated UCNP-based CORM prodrug delivery system for targeted cancer gas therapy.

1. Introduction

Cancer is the second leading cause of deaths worldwide. Recent investigations have demonstrated that cancer gas therapy is one potential approach for cancer treatment. The gaseous molecules, including nitric oxide (NO), carbon monoxide (CO) and hydrogen sulphide (H_2S), are known as gasotransmitters that are involved in many key biological processes [1–5]. They are endogenously generated to regulate important functions within specific cellular and molecular targets [6]. Specifically, CO is produced by the action of haem oxygenase 2 and inducible haem oxygenase 1 enzyme, and its key anticancer mechanism is to elevate the reactive oxygen species (ROS) level in mitochondria and inhibit mitochondrial respiration [7–11]. CO possibly inhibits cytochrome *c* oxidase, the terminal electron acceptor in the respiratory chain of mitochondria and enhances the level of Interleukin 10 (IL-10) [12–15]. CO binds tightly to the haemoglobin of red blood cells to form carboxyhemoglobin and produces a pseudo-hypoxic state in cells. This makes CO an interesting gasotransmitter for therapeutic purposes [16,17].

Several strategies have been devised to make these gases transportable within biological systems without diffusing to undesirable organs and tissues [18]. For example, Motterlini et al. pioneered the relevant research and successfully packaged CO gases into stable molecular compounds [19]. Recently, stimuli-responsive CO-releasing molecules (CORMs) have been synthesized by virtue of the preferential affinity of CO towards transition metals as transition metal carbonyl complexes containing several CO molecules (2-10 CO) [17,20–22]. These compounds are designed to be responsive to pH change, enzyme, thermal energy, light or oxidation to release the conjugated CO [19,23]. The latest nanotechnology advances have proven that novel nanodelivery systems can be engineered to deliver these metal-complex gaseous pharmaceutical agents [24,25] with high specificity to ensure that the absorption, distribution, metabolism, excretion and toxicity (ADMET) are well controlled for cancer therapy [26].

Over the past decade, nanodelivery systems have been extensively explored in biomedical fields for diagnosis and treatment of diseases. The nanoparticle systems have unique properties, which are able to

* Corresponding authors.
E-mail addresses: r.zhang@uq.edu.au (R. Zhang), gordonxu@uq.edu.au (Z.P. Xu).

https://doi.org/10.1016/j.ejpb.2020.11.014
Received 29 July 2020; Received in revised form 15 October 2020; Accepted 22 November 2020
Available online 1 December 2020

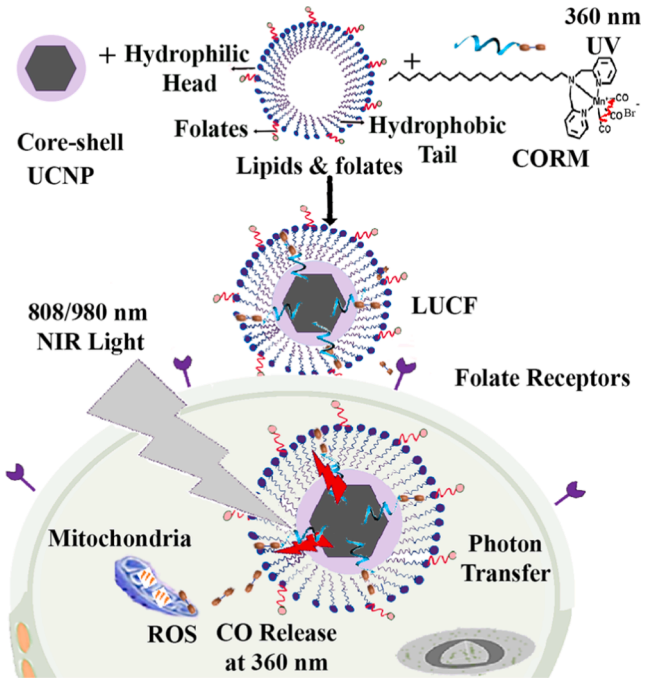

Scheme 1. Schematic diagram of CO release molecule (CORM) encapsulated in lipids with upconversion nanoparticles playing a mediatory role to absorb photons from a near infrared (NIR) light to produce a shorter wavelength photon capable of triggering CO release from CORMs. Folic acid was included in the lipid nanoformulation to improve cancer cell targeting.

increase drug solubility, enhance drug targeting, modulate release profile, load and deliver multiple drugs simultaneously [27,28]. In line with this, drug delivery researchers seek to package these CORMs into suitable nano-formulations for efficient delivery to specific targets in the body for treatment of cancer, anti-inflammation and cardiovascular diseases [29–31]. Attempts have been made to enhance the delivery of CORMs to targeted sites and control the release of CO molecules with internal and external stimuli [32,33]. Photoresponsive CORMs are the most popular one with the ability to absorb ultraviolet (UV) light to trigger the gradual release of CO within a specified period [34–36]. For example, Sakla et al. developed a lipid vesicle that was incorporated with amphiphilic manganese carbonyl complexes capable of being released by a UV light at 365 nm (half-life = 26.5 min) [37]. In general, the challenge is typically related to the responsive release of CO and the use of harmful UV light with short penetration depth in animal and human studies, thereby limiting the clinical application of photo-responsive CORMs.

On the other hand, synthesizing CORMs that absorb around the near-infrared (NIR) region is not feasible since CO-metal coordination bonds are only broken with high energy photons (300–400 nm), thus successfully using NIR light for light-responsive release of CO molecules remains much more challenging. For instance, Wu et al. synthesized an MnCO-entrapped mesoporous polydopamine nanoparticle with a characteristic photothermal property for CO release. They partially relied on the intrinsic property of H_2O_2 that is enhanced by NIR light to aid CO release [38]. Li et al. also produced a Prussian blue (PB) light responsive nanosystem to release CO via a bioreductive chemotherapeutic effect by activating Tirapazamine (TPZ) in the hypoxic environment. The PB effectively converts NIR light energy to heat to help release CO molecules [39]. Similarly, Yao et al. also produced a doxorubicin loaded Mn-carbonyl modified Fe (III)-based metal organic framework coated with PEGylated magnetic carbon nanoparticles. The magnetic carbonyl hybrids were incorporated to produce a photothermal effect that converts 808 nm NIR light to heat for CO release. A high power laser irradiation (3.0 W/cm^2) successfully heated the system for CO release [40]. These methods rely on the ability of the photothermal agent to heat up the nanosystem for CO release. Such a high laser power may hurt the skin directly and over-heat the tissue, causing damage in clinical practice. It is thus more ideal to control CO release by NIR laser *via* transformation to UV light within the nanodelivery system under relatively mild conditions.

This research aims to prove that a rationally designed nanoplatform is capable of harnessing and converting NIR to UV light to trigger CO release from CORM in a sustainable pattern, which carries and protects the gaseous prodrug (CORM) for enhanced cellular delivery. As illustrated in Scheme 1, the nanoplatform is constructed as lipid-coated upconversion nanoparticles (UCNPs) loaded with an amphiphilic manganese carbonyl complex prodrug in the lipid bilayer. Herein, UCNPs are designed with a core-shell structure ($NaYF_4$: Yb, Tm @$NaYF_4$:Nd) capable of absorbing and converting 980 or 808 nm NIR to UV–Vis lights. The folic acid (FA) conjugated with lipid molecules on the nanoparticle surface is used for targeted and enhanced delivery to cancer cells [41]. Upon cellular uptake, 808 or 980 nm NIR light is absorbed by UCNPs and converted to UV light that breaks Mn-CO bonds and releases CO molecules for therapeutic action. Our experimental data have demonstrated that (1) such a nanoplatform was successfully constructed and optimized; (2) the optimized nanoplatform efficiently converted 808 or 980 NIR to 360 nm UV light and controllably released CO; (3) this nanoplatform was effectively taken up by HCT116 cancer cells, in particular conjugated with the targeting ligand FA; and (4) the internalized nanoplatform induced the apoptosis of cancer cells via ROS overgeneration by released CO within the cells upon NIR irradiation. Thus, this work demonstrates a novel UCNP-based nanoplatform that controllably releases CO molecules for anti-cancer therapeutic action under biofriendly NIR irradiation.

2. Methodology

2.1. Materials

Lanthanides chloride hexahydrate ($TmCl_3{\cdot}6H_2O$, $NdCl_3{\cdot}6H_2O$, $YCl_3{\cdot}6H_2O$, $YbCl_3{\cdot}6H_2O$), ammonium fluoride (NH_4F), oleic acid (99% purity), oleylamine, and 1-octadecene were obtained from Sigma Aldrich. Sodium hydroxide (NaOH) was obtained from Chem-Supply. Cholesterol, 1,2-dioleoyl-*sn*-glycero-3-phosphocholine (DOPC), 1,2-dioleoyl-*sn*-glycero-3-phosphate (DOPA), 1,2-distearoyl-*sn*-glycero-3-phosphoethanolamine-N-(polyethylene glycol)-2000 (DSPE-PEG) and 1,2-dioleoyl-*sn*-glycero-3-phosphoethanolamine-N-(lissamine rhodamine B sulfonyl) (18:1 Liss Rhod PE), and 1,2-distearoyl-*sn*-glycero-3-phosphoethanolamine-N-[folate (polyethyleneglycol)-2000 (DSPE-PEG-FA) were obtained from Avanti Polar Lipids, USA. Dulbecco's Modified Eagle Medium (DMEM) and fetal bovine serum (FBS) were purchased from Gibco, USA. DCFH-DA ROS assay kit was purchased from Promokine. All other chemicals used were obtained from Merck KgaA (Darmstadt, Germany) and were of HPLC or analytical grade.

2.2. Synthesis of core-shell upconversion nanoparticles (UCNPs)

Core UCNPs ($NaYF_4$:Yb,Tm) were first synthesized using the thermal decomposition method. Under nitrogen gas atmosphere, $YCl_3{\cdot}6H_2O$ (0.795 mmol), $YbCl_3{\cdot}6H_2O$ (0.2 mmol) and $TmCl_3{\cdot}6H_2O$ (0.005 mmol) in a three-neck round bottom flask were dissolved with 6 mL of oleic acid (OA) and 15 mL of 1-octadecene (ODE) at 150 °C for 60 min. Upon cooling to room temperature, 10 mL of methanol solution containing 0.148 g of ammonium fluoride (NH_4F) and 0.1 g of sodium hydroxide (NaOH) was added. The mixture was stirred for another 60 min at room temperature, and then slowly heated to 120 °C for 30 min to get rid of methanol. The temperature was then rapidly increased to 310 °C for 90 min. After cooling down to room temperature, 10 mL of ethanol was added to precipitate the UCNPs. The formed UCNPs were then washed with methanol, ethanol and cyclohexane three times. The synthesized

UCNPs were dispersed in 10 mL of cyclohexane and stored at 4 °C for subsequent use.

The shell nanocrystal seeds (α-$NaYF_4$:Nd) (2 mmol) were prepared with the same thermal decomposition procedure. Typically, $YCl_3{\cdot}6H_2O$ (1.4 mmol) and $NdCl_3{\cdot}6H_2O$ (0.6 mmol) were magnetically dissolved in 12 mL of OA, 6 mL of oleylamine (OM) and 20 mL of ODE at 150 °C for 60 min. After cooling down to room temperature, methanol solution (10 mL) containing 0.296 g NH_4F and 0.2 g NaOH was added and the slurry was stirred at room temperature for another 30 min. Then, the reaction mixture was heated to 120 °C for 30 min to remove methanol, followed by heating to 290 °C for 30 min to produce α-$NaYF_4$:Nd. The resultant α-$NaYF_4$:Nd seeds obtained were dispersed in cyclohexane (2.0 mmol in 10 mL).

The core-shell nanoparticles ($NaYF_4$:Yb,Tm@$NaYF_4$:Nd) were synthesized by coating $NaYF_4$:Yb,Tm cores with α-$NaYF_4$:Nd nanocrystal seeds as follows: $NaYF_4$:Yb,Tm (2 mL/0.2 mmol) cores stocked in cyclohexane were magnetically mixed with OM (1 mL), OA (5 mL) and ODE (8 mL). α-$NaYF_4$:Nd shells to be used for the coating were processed by replacing cyclohexane with 1.5 mL of OM, 7 mL of OA and 11.5 mL of ODE by heating to 110 °C for 30 min under nitrogen gas. Upon heating the core nanoparticles to 303 °C, the $NaYF_4$:Yb,Tm core was quickly injected with 0.3 mL of α-NaYF4:Nd nanocrystal seeds using a syringe, followed by the addition of 0.2 mL every 10 min until the desired core: shell mass ratio (1:0.25, 1:0.5, 1:0.75 or 1:1) was achieved. After the last injection, the mixture was kept at 303 °C for 30 min to obtain the final core-shell $NaYF_4$:Yb,Tm@$NaYF_4$:Nd UCNPs. The precipitate was collected, washed and re-dispersed in cyclohexane using the same procedure for synthesizing core UCNPs.

2.3. Synthesis of lipid nanoformulations

The CORM was synthesised according to a previously reported procedure [37]. Lipid and CORM coated UCNP nanoformulations were prepared using thin-film hydration method. Firstly, for lipid-coated UCNPs with folates (LUF), 0.75, 1, 1.25, 1.5 or 3 mg of the lipid mixture (DOPC: DOPA: Cholesterol: DSPE-PEG: DSPE-PEG-FA) at a molar ratio of 40:40:10:5:5 was dissolved in chloroform (3 mL). Core-shell UCNPs (5 mg) were added to the lipid mixture in chloroform. The mixture was stirred for 4 h and sonicated in an ultrasonic water bath for 10 min. The organic solvent was slowly removed under reduced pressure in a rotary evaporator at 40 °C. The resultant thin film was dried in a vacuum oven overnight to ensure complete removal of traces of organic solvents. The thin film was then added with 2 mL of HEPES buffer (pH 7.4, 10 mmol) and stirred at 45 °C for 3 h. The mixture was centrifuged at 30,000*g* (4 °C) and the pellet was washed and redispersed in 1 mL of HEPES buffer. The lipid formulation (LUF) was finally sonicated for 20 min in an ultrasonic water bath, and stored at 4 °C for further analysis and use.

A similar procedure was carried out in the dark to prepare the CORM-encapsulated formulation with folates (LUCF) and Rhodamine-B-encapsulated (RhB) nanoparticles (Lipid/UCNP/RhB/FA (LURF)). Specifically, powdered CORM (0.3, 0.7, 1.2 or 2 mg) was added to the mixture of core-shell UCNPs (5 mg) and lipids (1.5 mg), followed by the same thin-film hydration method to obtain LUCF, LUR and LURF in HEPES buffer. For the preparation of LURF, the same process was employed by replacing CORM with 18:1 Liss Rhod PE (30 μg).

2.4. Characterization

The photoluminescence (PL) of various UCNPs were determined using 1 mL cyclohexane solution containing 5 mg of UCNPs in a quartz cuvette in a spectrometer with the excitation wavelength of 980 and 808 nm at 1 W/cm^2. The phase purity of the lyophilized core-shell UCNPs was examined by powder X-ray diffraction (Bruker D8 Advance MKII XRD) using Cu Ka radiation (λ = 1.5406 Å). The size and morphology of UCNPs and lipid-coated UCNPs were imaged in a Hitachi HT7700A transmission electron microscope (TEM) operated at 80 kV. STEM imaging (Hitachi HF500 Cs-STEM/TEM) was also performed on the core-shell UCNPs while energy-dispersive X-ray spectroscopy (EDS) was simultaneously performed to confirm the existence of lanthanide elements. The lipid-coated UCNPs were stained with 1% phototungsten acid (PTA) to observe the lipid coating on the particle surface in TEM images.

Dynamic light scattering (DLS) was employed to determine the particle size distribution and the zeta potential of LUF and LUCF in a Nano-ZS Zetasizer (Malvern Instruments). The particle size distribution and the zeta potential were measured every 2 days (up to 12 days) to examine the colloidal stability of the nanoformulations. The Fourier Transform Infrared (FTIR) spectra of nanoparticles were recorded with a Thermo Scientific Nicolet 6700 FTIR spectrophotometer. The UV-absorbance spectra of some UCNPs were also measured by a Shimadzu UV–Vis 2450 spectrophotometer. The LUCF samples were analyzed for C, H and O contents in a Thermo Scientific FLASH 2000 CHNS/O Analyzer.

The amount of pro-drug CORM encapsulated in LUCF formulation was calculated by determining the content of Mn element in the formulation via inductively coupled plasma-mass spectroscopy (ICP-OES) analysis. The drug (CORM) loading and encapsulation efficiency were calculated by the following equations:

$$\text{Drug loading (DL : \%)} = (\text{Mass of CORM in lipids})/(\text{LUCF Mass}) \times 100\%$$

$$\text{Entrapment efficiency (EE : \%)} = (\text{Drug loaded})/(\text{Drug initially added}) \times 100\%$$

2.5. In vitro CO release upon NIR irradiation

A CO fluorescence probe (COFP) dissolved in DMSO was employed to quantify the *in vitro* release of CO. An amount of LUCF formulation containing 100 μmol of CORM in HEPES buffer was added to the CO fluorescence probe (10 μmol in DMSO). The quartz cuvette containing the mixture was sealed with parafilm throughout the experiment to prevent the possible escape of CO from the test mixture. After irradiation with 808 or 980 nm NIR light (0.25, 0.5 or 1 W/cm^2 for 5 min), the fluorescence intensity of COFP (λ_{em} = 520 nm) at specific predetermined time intervals was recorded upon excitation (λ_{ex} = 440 nm).

2.6. Cell culture

Human colorectal carcinoma cell line (HCT116), murine melanoma cell line (B16F0), human breast cancer cell line (MCF-7) and human immortalized cervical cancer cell line (HeLa Cells) were grown in 90% DMEM or RPMI medium (for murine breast cancer cell lines (4T1)) supplemented with 10% FBS 100 U/mL penicillin, and 100 mg/mL streptomycin. Exponentially growing cultures were maintained in a humidified chamber containing 5% CO_2 at 37 ℃ throughout the cell studies.

2.7. Cellular uptake of lipid formulations

Confocal laser scanning microscopy (CLSM) and fluorescence spectroscopy were employed to examine the cellular uptake of lipid nanoformulation (LURF) by HCT116 cells using the synthesized Rhodamine B-lissamine lipid with desirable characteristics as a fluorescence probe (Table S3). The cells were seeded at a density of 1.5×10^5 cell/well in a 48-well plate and cultured for 24 h. First, the dose-dependent uptake of HCT116 cells for 3 h was determined at different formulation concentrations (ranging from 0 to 40 μg/mL). The fluorescence intensity of treated cells in PBS was determined with Tecan Infinite M200 PRO

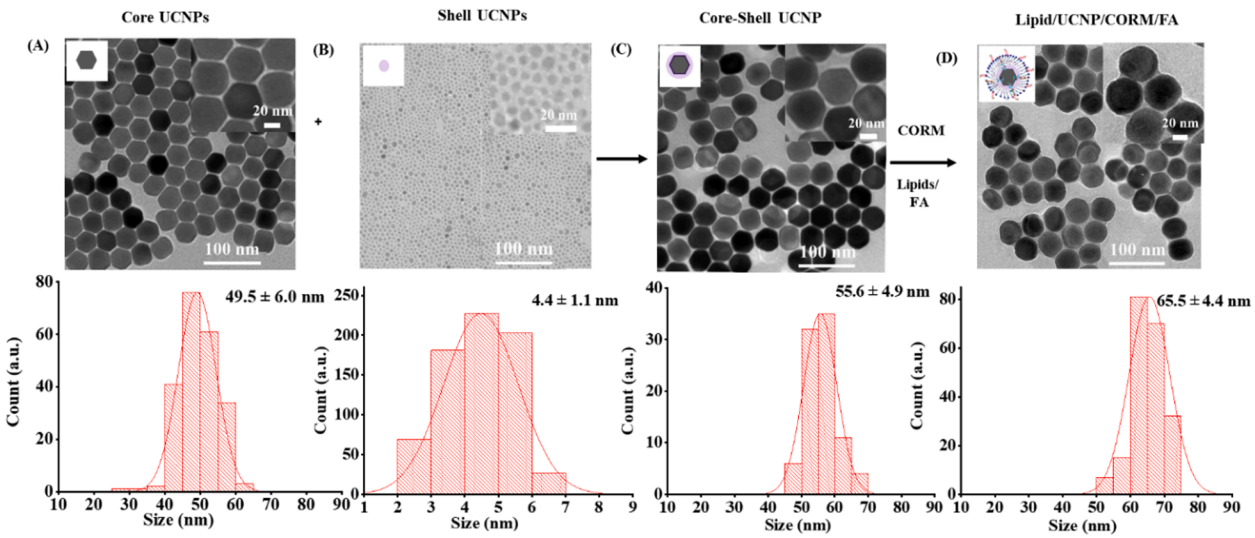

Fig. 1. Morphology and particle size distribution of UCNPs. TEM imaging showing the morphology and particle size distribution of (A) $NaYF_4$:Yb,Tm core; (B) $NaYF_4$:Nd shell UCNPs; (C) core-shell (1:0.5) $NaYF_4$:Yb,Tm@$NaYF_4$:Nd nanoparticles; and (D) Lipid/UCNP/CORM/FA (LUCF) with lipid coating around the core-shell UCNPs after staining with 1% PTA.

Multimode Microplate Reader (Switzerland) at λ_{em} = 583 nm upon excitation at λ_{ex} = 550 nm. The cellular uptake of LURF nanoparticles (20 μg/mL) by HCT116 cells was investigated at different time points (1, 2, 4, and 8 h) with Leica SP8 CLSM. After incubating the cells in culture media at 37 ℃ for the required period in the dark, the media with UCNPs were removed and the cells washed thrice with PBS, followed by staining with DAPI for imaging. The FA-enhanced uptake was also assessed at 8 h with LUR (without FA) and LURF (with FA) (Table S3).

2.8. Cell viability assay

HCT116 cells (5×10^3 cell/well) were seeded in a 96-well plate in 200 μL of culture medium after incubation for 24 h. The cells were exposed to 200 μL of FBS-free media containing various concentrations of LUCF and LUF nanoparticles (0–200 μg/mL) and incubated in the dark to assess their general cytotoxicity. After 3 h incubation, the media containing nanoparticles were replaced with fresh media, and the cells were treated with NIR light (808 nm, 1 W/cm^2) for 5 min. The cells were further incubated for a total of 48 h. MTT solution (20 μL, 5 mg/mL) was then added to each of the wells and the cells were incubated for 4 h. The medium was removed and the formazan product from MTT was dissolved in 100 μL of dimethyl sulfoxide (DMSO). The absorbance was measured at 570 nm in relation to the reference at 670 nm using Tecan Infinite M200 PRO Multimode Microplate Reader (Switzerland). The same assay was applied to B16F0, 4T1, MCF-7, and Hela cells. The cell viability was expressed as a percentage of the untreated cells (control group) and calculated with the equation:

$$\text{Cell viability } (\%) = ([OD]_{test}/[OD]_{control}) \times 100\%,$$

where $[OD]_{test}$ is the optical density of test sample and $[OD]_{control}$ that of the control group.

2.9. Intracellular CO and ROS detection

COFP was used to detect the release of CO in HCT116 cells. Cells were seeded in a 48-well plate at a density of 2×10^4 cell/well. After incubation at 37 °C for 24 h, the cells were incubated in media containing COFP (10 μM) and LUF or LUCF nanoparticles (50 μg/mL) for 3 h in the dark. The cell culture media containing nanoparticles and probes were then removed, and the treated cells were carefully washed with PBS for three times. Then, fresh culture media was added to each well, followed by irradiation with 808 nm NIR at 1 W/cm^2 for 5 min. The cells were further incubated for 3 h before washing three times with PBS. The cells were collected by treating with trypsin via centrifugation. The cells were resuspended in 150 μL of FACS buffer for flow cytometry analysis with Beckman Coulter FC 500. Untreated cells and cells treated with only COFP were included as control groups.

The intracellular ROS was performed by incubating cells with 2′-7′-dichlorodihydrofluorescein diacetate (DCFH-DA) (10 μmol) analysis kit. HCT-116 cells in DMEM were seeded in a 48-well plate at a density of 2×10^4 cell/well. After incubation at 37 °C for 24 h, the cell culture media were replaced with media containing nanoparticles (50 μg/mL) for 3 h. The media were replaced with fresh ones and the cells were irradiated with 808 nm NIR laser at 1 W/cm^2 for 5 min. After further incubation in the dark for 3 h, the cells were collected, washed thrice, harvested with 150 μL FACS buffer and analyzed by flow cytometry to detect DCF fluorescence (λ_{ex} = 488 nm). Untreated cells and cells treated with only DCFH-DA were included as control groups.

2.10. Statistical analysis

The data are presented as the mean ± standard error from at least triplicate experiments performed in a parallel manner unless otherwise stated. The differences among the groups were analyzed using one-way analysis of variance (ANOVA), and the significance was indicated as *$p < 0.05$, **$p < 0.01$, and ***$p < 0.001$.

3. Results and discussion

3.1. Characteristics of synthesized UCNPs

The core UCNPs ($NaYF_4$: Yb, Tm) were synthesized with three lanthanide elements, namely Yttrium (Y) as the $NaYF_4$ matrix, Ytterbium (Yb) as the main sensitizer and Thulium (Tm) as the emitter. As compared to other emitters like Erbium, Tm is capable of emitting photons around 360 nm after absorbing NIR light (808 or 980 nm) from sensitizer Yb. The core $NaYF_4$:Yb,Tm UCNPs had an average size of 49.5 ± 6.0 nm (Fig. 1A). In order to endow the core UCNPs with 808 nm NIR-light absorbing properties, the cores were coated with the UCNP nanoshells containing Nd element ($NaYF_4$:Nd), which were prepared as nanodots (4.4 ± 1.1 nm, Fig. 1B). As shown in Fig. 1C, the particle size increased from about 49.5 to 55.6 nm upon coating of shell nanodots (core:shell mass ratio: 1:0.5) and kept increasing with the amount of

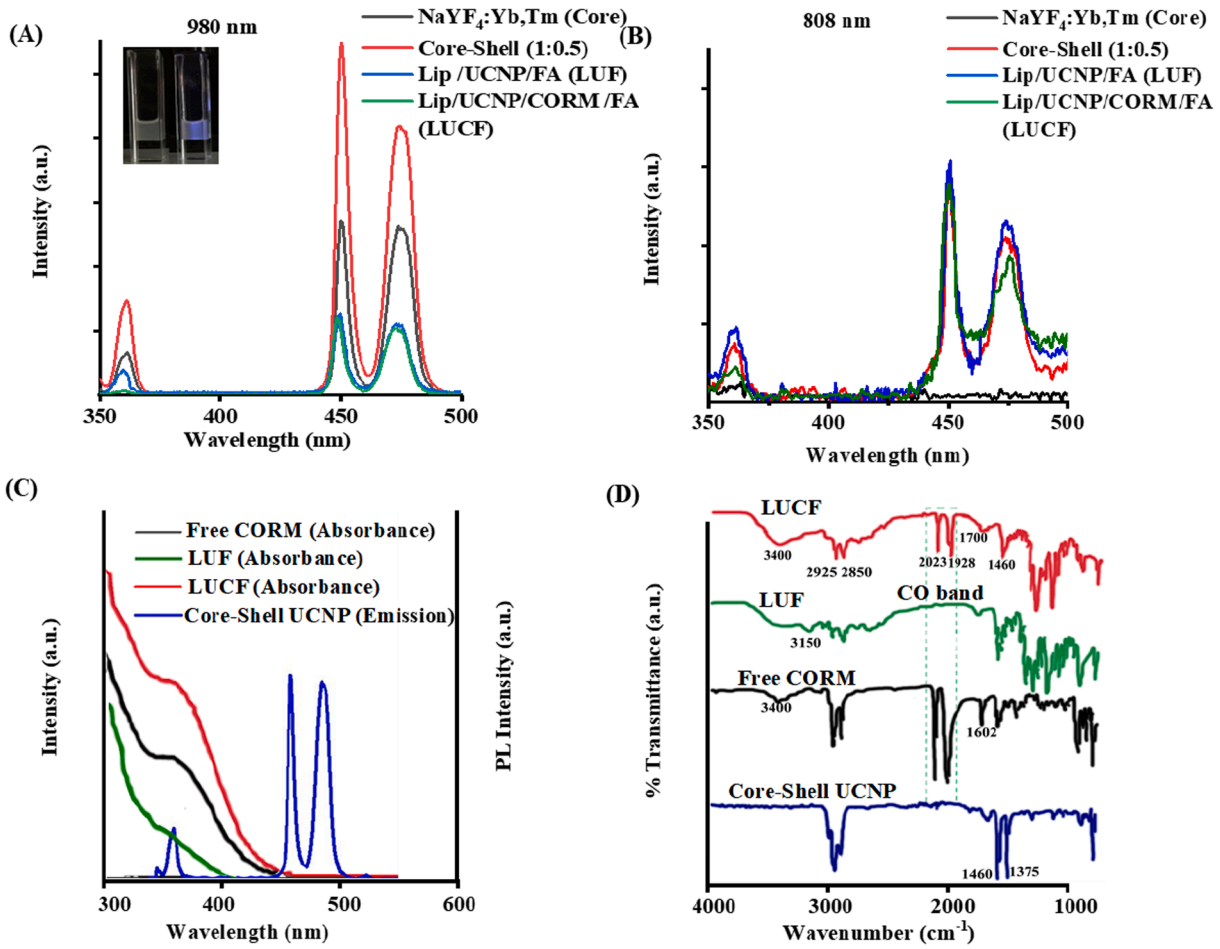

Fig. 2. Characterizations of photo-physical properties and surface of UCNP-based nanoparticles. PL spectra of core $NaYF_4$:Yb,Tm, core-shell $NaYF_4$:Yb,Tm@ $NaYF_4$: Nd nanoparticles, LUF, and LUCF under excitation at (A) 980 nm (Inset: Appearance of LUCF under ambient light and under NIR 980 nm light) and (B) 808 nm; (C) the absorption of LUF, LUCF and free CORM and the overlapping between the absorption of LUCF/CORM and the emission of core-shell UCNP at the UV region; (D) FTIR spectra of core-shell UCNPs, CORM, LUF and LUCF nanoparticles showing their respective characteristic vibrations.

shell nanodots added. The size increase of other core-shell UCNPs (1:0.25, 1:0.75 and 1:1) was also evidenced in TEM images (Fig. S1A–D).

The typical XRD pattern (Fig. S1E) confirms the formation of hexagonal UCNPs ($NaYF_4$ and its likes) when compared with known ones retrieved from JCPDS No. 27–0699. STEM imaging and EDS analysis for 1:0.5 and 1:1 core-shell UCNPs show the difference in the lanthanide composition, indicating coating of shell nanodots on the surface of core UCNPs (Fig. S2). As expected, the coated shells (core:shell 1:0.5) increased the PL intensity at 360 nm upon excitation by both 808 and 980 nm NIR (Fig. 2A and B). Interestingly, the PL intensity at 360 nm was peaked at the core-shell mass ratio of 1:0.5 (Fig. S3A and B), due to the doping of a suitable amount of Nd in the shell. A high amount of Nd (e.g. the core-shell mass ratio of 1:1) may affect the composition and decrease the Tm emitting at the UV–Vis region, while reversely, a very thin shell on the core UCNPs (such as the core-shell mass ratio of 1:0.25) may not be enough to fully protect the core surface against PL quenching from solvents [42]. Thus, a moderate amount of the shell (such as 1:0.5 mass ratio) balances the effect on the core composition and solvent quenching, leading to the strongest PL signal. Therefore, UCNPs with the core:shell mass ratio of 1:0.5 were selected as the basis for the UCNP-mediated delivery system in this work (Fig. 2A and B).

3.2. Characteristics of lipid-coated CORM-loaded UCNP nanoformulation

As summarized in Table S1, LUF nanoformulations, i.e. lipid-coated UCNPs with targeting FA were made successfully. The Z-average particle size (152–163 nm) indicated that the amount of lipids and CORMs did not significantly affect the particle size distribution, but slightly influenced the zeta potential. As shown in Fig. S4A and B, a combination of 5 mg of core/shell UCNPs and 1.5 or 3.0 mg of lipids significantly enhanced the PL intensity at 360 nm. It seems that 5 mg UCNPs and 1.5 mg lipids (DOPC: DOPA: Cholesterol: DSPE-PEG: DSPE-PEG-FA at a molar ratio of 40:40:10:5:5) formulated smaller lipid-coated UCNPs with a relatively less amount of lipids used. Therefore, 1.5 mg of lipids was selected as the optimal amount for UCNP encapsulation. In this experiment, as-prepared core-shell UCNPs were not dispersible in HEPES buffer, but coating lipids bestowed a characteristic hydrophilic property to oleic acid-capped core-shell UCNPs. Thus lipid-coated UCNPs showed a good dispersion in HEPES buffer, and maintained the high PL property.

Further, a certain amount of CORMs was included into lipid-coated UCNPs in the formulation (LUCF). As listed in Table S2, the LUCF nanoformulations had the average particle size of 154–162 nm, with the Zeta potential from −1.0 to 12 mV. The positive charge of CORMs may render the net surface charge of hybrid LUCFs positive. The PL spectra of LUF and LUCF formulations in HEPES buffer were determined and compared to the core and core-shell UCNP nanoparticles dispersed in cyclohexane. As shown in Fig. 2A, B the relative intensity indicated that UCNPs were encapsulated successfully and produced PL signals in aqueous suspensions. Significantly, the PL intensity of 360 nm was influenced with respect to the nominally encapsulated amount of CORM

Table 1
Summary of LUF and LUCF particle characteristics in HEPES indicating the DLS properties, and the drug loading efficacy and yield.

Samples	Hydrodynamic diameter (nm)	Zeta potential (mV)	Polydispersity index (PDI)	Drug loading (%)	Yield (%)
Lip/UCNP/FA (LUF)	153.9 ± 2.8	−5.1 ± 2.9	0.25 ± 0.15	–	53
Lip/CORM/UCNP/FA (LUCF)	158.3 ± 3.9	−0.9 ± 0.2	0.24 ± 0.11	18.1	51

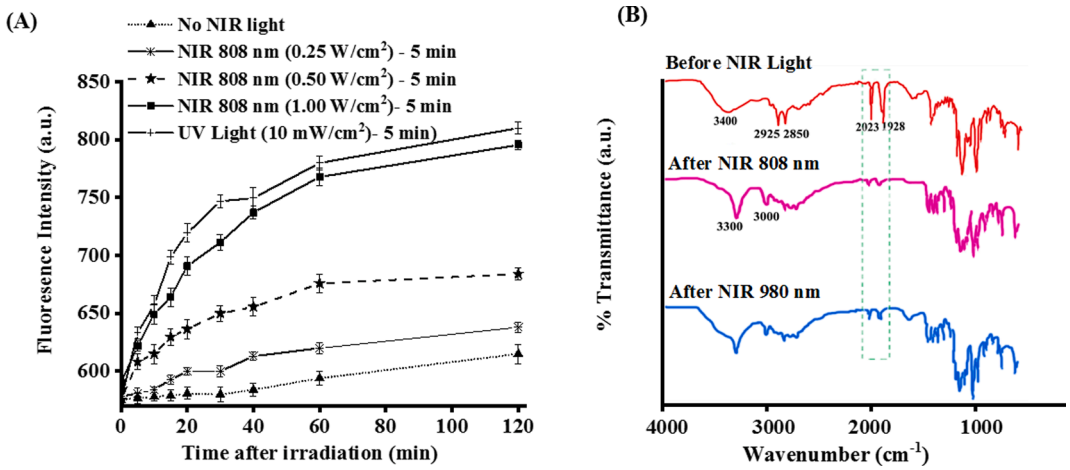

Fig. 3. NIR-triggered release of CO from lipid-coated CORM-loaded UCNPs. (A) CO release profile of LUCF in the presence of CO fluorescent probe in HEPES buffer at λ_{ex} = 440 nm and λ_{em} = 520 nm before and after light irradiation for 5 min at 0.25/0.5/1 W/cm^2; (B) FTIR spectra of LUCF indicating the characteristic change in CO vibrations (2023 and 1928 cm^{-1} upon release with NIR 980 and 808 nm light for 5 min at 1 W/cm^2.

[43] (Fig. S5A and B). As seen in Fig. 2A, the emissions around 450 and 475 nm were maintained for LUF, but the high-energy UV peak (360 nm) was nearly eliminated in LUCF (Fig. S7) and the relative PL intensity (i.e. the ratio of 360:450 nm peak intensity) decreased obviously with the CORM amount increasing from 0.3 to 2.0 mg because CORM and LUCF absorb the UV light in 340–380 nm (Fig. 2C). In order for LUCF to absorb more fluorescent UV light emitted from UCNPs for mediated CO release, LUCF nanoparticles with the lipid/UCNP/CORM mass ratio of 1.5:5:2.0 was selected. This formulation did demonstrate superior PL overlapping at 360 nm (Fig. 2C), having a high encapsulation efficiency (77%) with 18.1 wt% of CORMs loaded (Table 1), i.e. 2.26 wt% CO in the total nanoparticle formulation.

Moreover, DOPC: DOPA: cholesterol: DSPE-PEG: DSPE-PEG-FA ratio (40:40:10:5:5) was selected as it exhibited a negative zeta potential in comparison with that of the lipid composition (45:35:10:5:5) (Table S2). As shown in Fig. 1D, the TEM image confirmed that the lipids were successfully coated on the UCNP surface when the morphology and appearance of lipid-free core-shell UCNPs and LUCF nanoformulations were compared after PTA staining. As further shown in Fig. 2D, oleic acid capping of core-shell UCNPs was confirmed with characteristic vibrations at 2850–2925 and 1460 cm^{-1} in the FTIR spectrum [44]. The coated lipids in LUF were also evidenced with the 'finger-print' signals in 800–1500 cm^{-1}. After successfully encapsulating CORMs in LUCF nanoparticles, two characteristic vibrations of CORMs at 2023 cm^{-1} and 1928 cm^{-1} [37] were also observed (Fig. 2D), suggesting that CORMs were well incorporated into the lipid-based delivery vehicles. The stability of the formulated CORM delivery system (LUCF) was also confirmed as the zeta potential (-1.0 to −1.2 mV) and the particle size (155–165 nm) were constant in the 12-day stability test (Fig. S6A). The stability of the formulation in acetate buffer (pH = 5.0) was also confirmed (Fig. S6B). As listed in Table S3, LURF and LUR were similar in size and had a similar Zeta potential (-1.3 ± 0.2). This formulation is thus suitable for the assessment of cellular uptake.

3.3. NIR-triggered CO release from LUCF nanoformulation

In order to demonstrate the *in vitro* release of CO, a CO fluorescence probe (COFP) was adapted to track the NIR light-induced CO release from LUCF in HEPES buffer according to a previously described fluorescence turn on mechanism [45]. As shown in Fig. 3A, irradiation with 808 nm NIR light for 5 min intensified the COFP's fluorescence gradually with the release time, which was also dependent on the NIR power density. It seemed that the CO release reached its maximal plateau within 1 h after irradiation for 5 min at 1 W/cm^2, which is similar to the release profile of CO from CORMs upon UV irradiation for 5 min at 0.01 W/cm^2. This UV irradiation is expected to release all CO from CORMs [46].

Table 2
Elemental analysis of carbon, hydrogen and nitrogen before and after light irradiation, representing the release of CO molecules.

Samples	Carbon (C) (%)	Hydrogen (H) (%)	Nitrogen (N) (%)
Before Light	34.38	6.15	3.99
980 nm Light	32.97	5.58	4.12
808 nm Light	32.62	5.57	3.90

The CO release was also confirmed with FTIR analysis before and after NIR-light irradiation. As shown in Fig. 3B, CO's characteristic vibrations at 2023 and 1928 cm^{-1} were significantly decreased upon irradiation with either 808 or 980 nm NIR for 5 min at 1 W/cm^2. Elemental analysis also confirmed the loss of CO molecules in the same samples used to record FTIR spectra. There was 1.4–1.7 wt% carbon (C) loss (Table 2) upon NIR irradiation. This C loss semi-quantitatively agreed with nearly all CO release from the sample. As LUCF contained 18.1 wt% CORM, which has 12.5 wt% CO (3 × 28/670.6), LUCF contained 2.26 wt% CO, i.e. 0.98 wt% C. This suggests that almost all loaded CO in LUCF was released under the selected irradiation condition, which is supported by the change of CO peaks' intensity in FTIR spectra (Fig. 3B).

3.4. Cellular uptake of nanoformulations

Different amounts of Rhodamine B-encapsulated lipid/UCNP

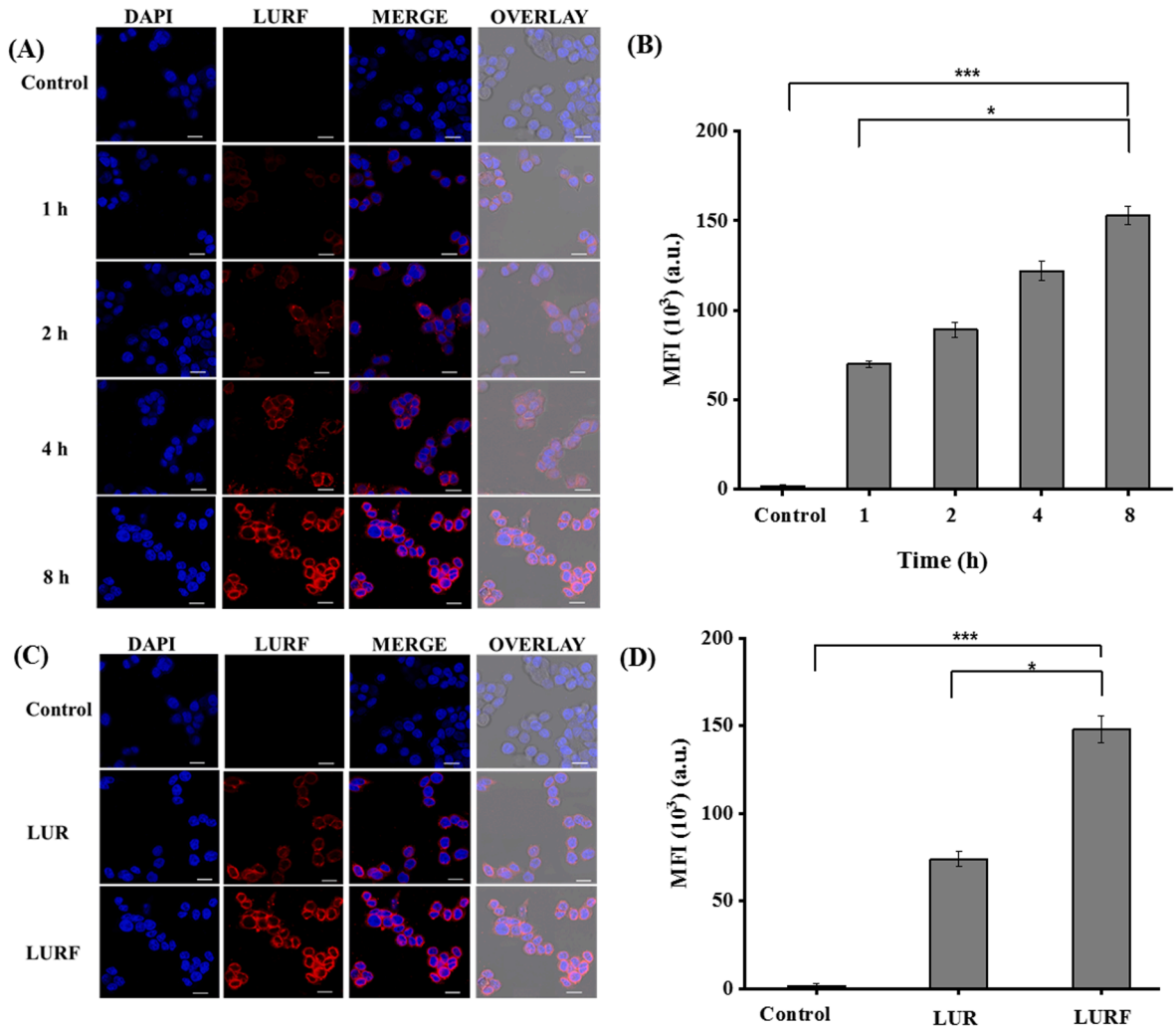

Fig. 4. Cellular uptake of lipid-coated UCNPs. (A) Fluorescence imaging and (B) flow cytometry analysis of HCT116 cells incubated with LURF for 1, 2, 4, and 8 h; (C) Cell uptake images of LURF and LUR nanoformulation after 8 h of incubation and (D) mean fluorescence intensity (MFI) of HCT 116 cells after 8 h of incubation with LURF and LUR nanoparticles.

nanoparticles with folates (LURF) or without folates (LUR) were used to assess the cellular uptake of nanoparticles at 3 h. As shown in Fig. S8A, the fluorescence of HCT116 cells increased with the dose of LUR and LURF in culture medium, indicating the cellular uptake of these nanoparticles is dose-dependent, as reported for many liposome nanoparticles [47]. Clearly, 20 μg/mL of the nanoformulations produced enough high mean fluorescence intensity (MFI) and fluorescence-positive cell percentage (40–70%), and was used to determine the time-dependent uptake profile. As shown in Fig. 4A, the uptake by HCT116 cells obviously increased with the incubation time as reflected by the gradual increase in red fluorescence of Rhodamine B. Relatively, the cellular uptake seemed much slower after 4 h as there was only ~ 20% increase in uptake by cells in 4–8 h (Fig. 4B).

Very obviously, FA conjugation on the nanoparticle surface (5% mol) significantly facilitated the cellular uptake (Figs. 4C, D and S8A), by nearly 100%, largely due to specific interactions of FA with its receptor overexpressed in HCT116 cancer cells [48,49]. This confirms the hypothesis that delivery of LUCF nanoparticles to cancer cells can be enhanced by specific targeting strategy via folate-folate receptor interactions. The mean fluorescent intensities (MFI) measured from CLSM images also confirmed the significant enhancement of LURF cellular uptake (Fig. 4C and D). Therefore, FA-conjugated LUCF nanoparticles were used in the cytoxicity test.

3.5. NIR-triggered cytotoxicity of nanoformulations

CO's therapeutic potential was determined at different CORM concentrations to confirm the proposed action of CO in several tumor cells. First, the cytotoxicity of the carrier nanoparticles (LUF) was assessed. As shown in Fig. 5A, LUF did not cause obvious HCT116 cancer cell death for 48 h, even at concentrations up to 200 μg/mL in culture medium with 808 nm NIR irradiation at 1 W/cm^2 for 5 min (conducted at 3 h post incubation), which was also observed in some other tumour cells, such as FA-positive MCF7, 4T1, B16, and HeLa cells (Fig. S8B). Previous reports indicate that surface-modified UCNPs are generally safer and do not cause significant toxicity to cells even though bare UCNPs are also considered biosafe [50]. Herein, encapsulating UCNPs with lipids may further reduce the cytotoxicity as the lipid layer shields UCNPs from direct interactions with different biological environments before reaching cell targets.

As shown in Fig. 5B, the cell viability of HCT116 decreased with the LUCF dose upon irradiation of either 980 or 808 nm NIR after 3 h uptake, and then continuous incubation for 48 h in total. Seemingly, two kinds of NIR lights generated a high cytotoxicity to cancer cells in a similar pattern, in consistence with the similar CO release behaviors upon irradiation with the respective lights (Fig. 3B). Both NIR lights induced 50% cell death at 20 μg/mL of LUCF. In comparison, the cytoxicity of LUCF nanoparticles without NIR irradiation seemed higher

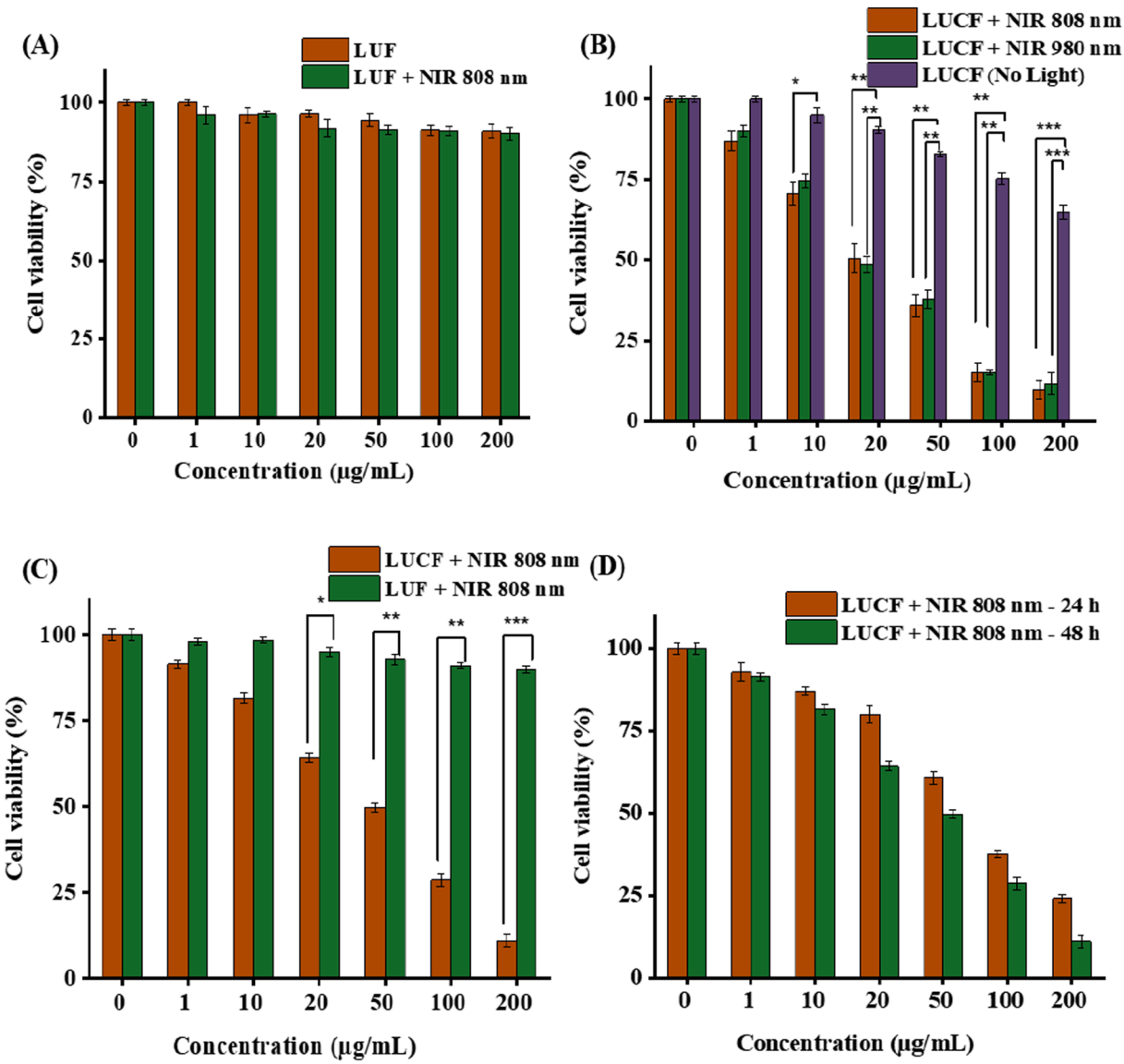

Fig. 5. Cytotoxicity of lipid-coated CORM-loaded UCNPs. (A) Cell viability assay of lipid-coated UCNPs (LUF) in HCT116 cells without light irradiation and with 808 nm NIR light and incubated without nanoparticle washing for 48 h; (B) Cell viability assay of LUCF with 808, 980 nm and no light after 48 h without removal of nanoparticles; (C) Cell viability assay of LUF and LUCF in HCT 116 cells irradiated with 808 nm NIR light and incubated for 48 h. LUCF was washed and replaced with fresh media after 3 h of incubation before light irradiation; (D) Cell viability assay of HCT-116 after 48 h of incubation compared to 24 h of incubation. NIR light irradiation performed after 3 h of incubation, and cells with nanoparticles were replaced with fresh media. NIR light irradiation was maintained at 1 W/cm^2 for 5 min throughout all experiments.

than that of nanocarriers (LUF, Fig. 5A and B). For example, the cell viability was 91.0 ± 0.9% and 75.2 ± 1.8% for LUF and LUCF at 100 μg/ml, respectively. The higher cytotoxicity of LUCF is probably attributed to the casual CO release caused by incidental lights in the lab and intrinsic H_2O_2 in cancer cells that may also cause CO release from CORMs loaded in the lipid layer of UCNPs.

Fig. 5C suggests that there was just a marginal increase in the cytotoxicity among cells incubated with nanoparticles without removal after three h. This suggests that CO released from nanoparticles in medium did not obviously contribute to apoptosis of HCT116 cells. As further shown in Fig. 5D, the cell viability slightly decreased when the second incubation time increased from 21 h to 45 h (total 24 h and 48 h, respectively), which suggests that CO-induced apoptosis is continued for 2 days after NIR irradiation.

Our nanoplatform performed much better than reported nanosystems in terms of the cell apoptosis and the irradiation condition. For example, our nanoplatform with the CO dosage of 2.26 μg/mL (100 μg/mL of total nanoparticles) reduced the cell viability to 37.6% and 28.6% upon 808 nm laser irradiation at 1 W/cm^2 for 5 min in 24 h and 48 h incubation, respectively (Fig. 5D). In contrast, Yao et al. reported that their nanoplatform with a characteristic NIR to heat conversion by a high-power laser (3 W/cm^2 for 3 min) only reduced the HCT116 cell viability to 90% at 1.1 μg/mL of CO in 24 h incubation [40]. In another study, Wu et al. utilized a photothermal nanoplatform at the doses of 100 and 200 μg/mL (i.e. CO dose of 43 and 86 μg/mL) to target HCT116 cells, which reduced the cell viability to about 78% and 30% with the NIR laser irradiation at 1 W/cm^2 for 5 min during 48 h incubation [38]. Therefore, the photoresponsive release of CO by the UV photons upconverted from irradiated 808 nm NIR via UCNPs enhanced the CO therapeutic efficacy.

Very similarly, LUCF nanoformulation also showed a dose-dependent cytotoxicity to other FA-positive cell lines (MCF7, 4T1, B16 and Hela cells) (Fig. S8C) while HCT116 seemed the most sensitive. This is probably because of specific characteristic properties related to

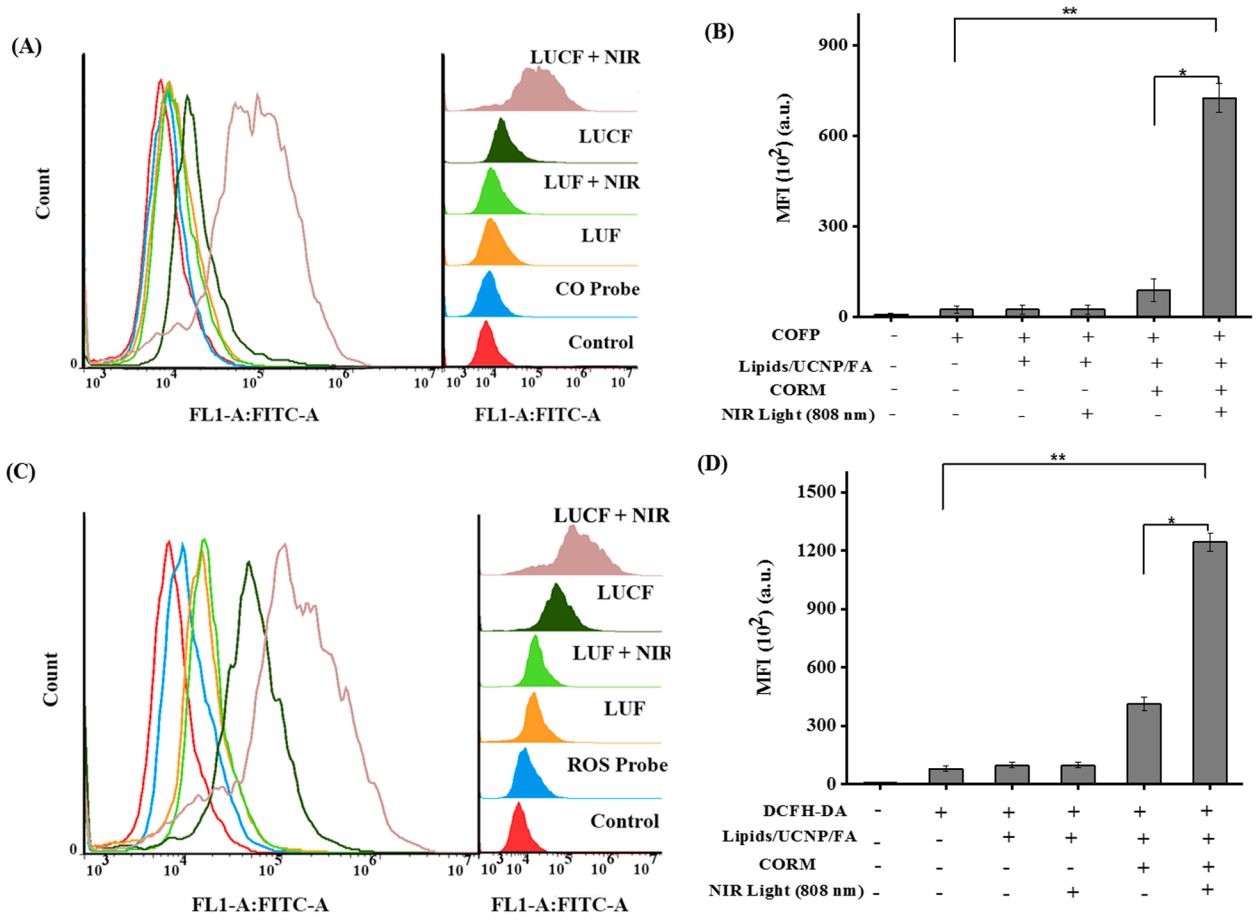

Fig. 6. Intracellular release of CO and generation of ROS. (A) Flow cytometry analysis and (B) mean fluorescence intensity for intracellular CO detection in HCT116 cells after incubation with LUCF nanoparticles and LUF (with/out NIR 808 nm light at 1 W/cm^2 for 5 min; (C) Flow cytometry analysis and (D) mean fluorescence intensity for ROS detection in HCT116 cells with LUCF and LUF (with/out 808 nm NIR light at 1 W/cm^2 for 5 min).

HCT116, such as AKt phosphorylation, which is ochestrated by CO molecules, directly targeting Akt signaling pathway present in most colorectal cancer growth [43,51].

3.6. Intracellular CO release and ROS generation

As clearly shown in Fig. 6A, CO was released internally in cells, as indicated by flow cytometry data. In particular, the cells treated with LUCF generated the highest amount of CO upon 808 nm irradiation (the highest bar in Fig. 6B), consistent with the NIR-triggered cytotoxicity (Fig. 5).

Similarly, DCFH-DA probe was employed to assess the level of ROS produced in the cytosol in accordance with the mechanism of action of CO molecules. As shown in Fig. 6C and D, the production of ROS in LUCF-incubated cells was enhanced significantly upon light irradiation. The ROS generation in LUCF-treated cells was well correlated with the amount of CO released in cells, as indicated by the high linear coefficient (R^2 = 0.9991) (Fig. S9C). These data suggest that an increase in CO release contributes to a higher level of intracellular ROS and enhances cancer cell apoptosis. As is well known, Cytochrome *c*, a heme protein released from mitochondria to the cytosol during apoptosis, is capable of oxidizing DCFH directly or indirectly via a peroxidase-type mechanism, forming fluorescent DCF. The increase in the DCF fluorescence during apoptosis of cells is frequently associated with enhanced oxidant production [52]. Therefore, the released CO molecules in cells facilitate ROS production and orchestrate cancer cell death.

Therefore, our nanodelivery platform has achieved the NIR-to-UV conversion and induced the release of CO from CORM for efficient cancer gas therapy. This mechanism is different from other similar investigations, which heavily rely on photothermal conversion with either a longer period of irradiation or a high laser power to increase the systematic temperature to a level for CO release. Of course, further in vivo studies are necessary to clearly ascertain their effects on various biological environments, and the long-term biological effects of lipid-coated UCNPs and their interaction with the reticuloendothelial system should be further investigated for future preclinical and clinical applications.

4. Conclusions

This research has demonstrated the controlled CO release with a suitable NIR trigger for cancer gas therapy. We successfully incorporated CORM, a CO-containing metal complex, into a biocompatible lipid delivery vehicle containing UCNPs as the cores capable of triggering CO release upon NIR light irradiation. The synthesized core-shell UCNPs were capable of converting NIR to UV, and the converted 360 nm UV light triggered the release of almost all CO molecules from CORM upon irradiation of 808 or 980 nm NIR at 1.0 W/cm^2 for 5 min. The released CO molecules efficiently induced cell apoptosis mainly due to generation of ROS. Thus, this research has proven the concept that CO release can be locally controlled with the NIR light via UCNPs to induce cancer cell apoptosis as a cancer gas therapy, which will be tested in the next in vivo experiment.

Declaration of Competing Interest

The authors declare that they have no known competing financial interests or personal relationships that could have appeared to influence the work reported in this paper

Acknowledgements

The authors acknowledge financial supports from Australian Research Council (ARC) Discovery Projects (DP170104643 and DP190103486). Y. O-D. gratefully acknowledges the Australian Government Research Training Program Scholarship (RTP). The authors also give thanks to facilities and the technical assistance of the Australian Microscopy & Microanalysis Research Facility at the Centre for Microscopy and Microanalysis (CMM), Australian National Fabrication Facility (QLD Node) and Centre of Advance Imaging, The University of Queensland.

Appendix A. Supplementary material

Supplementary data to this article can be found online at https://doi.org/10.1016/j.ejpb.2020.11.014.

References

[1] W. Fan, B.C. Yung, X. Chen, Stimuli-responsive NO release for on-demand gas-sensitized synergistic cancer therapy, Angew. Chem. Int. Ed. 57 (2018) 8383–8394.
[2] C.R. Powell, K.M. Dillon, J.B. Matson, A review of hydrogen sulfide (H2S) donors: chemistry and potential therapeutic applications, Biochem. Pharmacol. 149 (2018) 110–123.
[3] M.R. Hellmich, C. Coletta, C. Chao, C. Szabo, The therapeutic potential of cystathionine beta-synthetase/hydrogen sulfide inhibition in cancer, Antioxid. Redox Signal. 22 (2015) 424–448.
[4] E.M. Bos, H. van Goor, J.A. Joles, M. Whiteman, H.G. Leuvenink, Hydrogen sulfide: physiological properties and therapeutic potential in ischaemia, Br. J. Pharmacol. 172 (2015) 1479–1493.
[5] A. Sparatore, G. Santus, D. Giustarini, R. Rossi, P. Del Soldato, Therapeutic potential of new hydrogen sulfide-releasing hybrids, Expert Rev. Clin. Pharmacol. 4 (2011) 109–121.
[6] M. Mojic, S. Mijatovic, D. Maksimovic-Ivanic, D. Miljkovic, S. Stosic-Grujicic, M. Stankovic, K. Mangano, S. Travali, M. Donia, P. Fagone, M.B. Zocca, Y. Al-Abed, J.A. McCubrey, F. Nicoletti, Therapeutic potential of nitric oxide-modified drugs in colon cancer cells, Mol. Pharmacol. 82 (2012) 700–710.
[7] C. Taille, J. El-Benna, S. Lanone, J. Boczkowski, R. Motterlini, Mitochondrial respiratory chain and NAD(P)H oxidase are targets for the antiproliferative effect of carbon monoxide in human airway smooth muscle, J. Biol. Chem. 280 (2005) 25350–25360.
[8] P. Kaczara, R. Motterlini, G.M. Rosen, B. Augustynek, P. Bednarczyk, A. Szewczyk, R. Foresti, S. Chlopicki, Carbon monoxide released by CORM-401 uncouples mitochondrial respiration and inhibits glycolysis in endothelial cells: A role for mitoBKCa channels, BBA 2015 (1847) 1297–1309.
[9] K. Srisook, S.S. Han, H.S. Choi, M.H. Li, H. Ueda, C. Kim, Y.N. Cha, CO from enhanced HO activity or from CORM-2 inhibits both O2- and NO production and downregulates HO-1 expression in LPS-stimulated macrophages, Biochem. Pharmacol. 71 (2006) 307–318.
[10] H. Soni, G. Pandya, P. Patel, A. Acharya, M. Jain, A.A. Mehta, Beneficial effects of carbon monoxide-releasing molecule-2 (CORM-2) on acute doxorubicin cardiotoxicity in mice: role of oxidative stress and apoptosis, Toxicol. Appl. Pharmacol. 253 (2011) 70–80.
[11] C.C. Lin, L.D. Hsiao, R.L. Cho, C.M. Yang, Carbon monoxide releasing molecule-2-upregulated ROS-dependent Heme oxygenase-1 axis suppresses lipopolysaccharide-induced airway inflammation, Int. J. Mol. Sci. 20 (2019).
[12] S. Akyol, S. Erdogan, N. Idiz, S. Celik, M. Kaya, F. Ucar, S. Dane, O. Akyol, The role of reactive oxygen species and oxidative stress in carbon monoxide toxicity: an in-depth analysis, Redox Rep. 19 (2014) 180–189.
[13] T.S. Lee, L.Y. Chau, Heme oxygenase-1 mediates the anti-inflammatory effect of interleukin-10 in mice, Nat. Med. 8 (2002) 240–246.
[14] R. Long, I. Salouage, A. Berdeaux, R. Motterlini, D. Morin, CORM-3, a water soluble CO-releasing molecule, uncouples mitochondrial respiration via interaction with the phosphate carrier, BBA 2014 (1837) 201–209.
[15] J. Lv, Y. Liu, S. Jia, Y. Zhang, H. Tian, J. Li, H. Song, Carbon monoxide-releasing molecule-3 suppresses tumor necrosis factor-alpha- and interleukin-1beta-induced expression of junctional molecules on human gingival fibroblasts via the Heme oxygenase-1 pathway, Mediators Inflamm. 2020 (2020) 6302391.
[16] C. Szabo, Gasotransmitters in cancer: from pathophysiology to experimental therapy, Nat. Rev. Drug Discov. 15 (2016) 185–203.
[17] R. Motterlini, L.E. Otterbein, The therapeutic potential of carbon monoxide, Nat. Rev. Drug. Discov. 9 (2010) 728–743.
[18] R. Foresti, J. Hammad, J.E. Clark, T.R. Johnson, B.E. Mann, A. Friebe, C.J. Green, R. Motterlini, Vasoactive properties of CORM-3, a novel water-soluble carbon monoxide-releasing molecule, Br. J. Pharmacol. 142 (2004) 453–460.
[19] R. Motterlini, B.E. Mann, T.R. Johnson, J.E. Clark, R. Foresti, C.J. Green, Bioactivity and pharmacological actions of carbon monoxide-releasing molecules, Curr. Pharm. Des. 9 (2003) 2525–2539.
[20] N.E. Brückmann, M. Wahl, G.J. Reiß, M. Kohns, W. Wätjen, P.C. Kunz, Polymer Conjugates of Photoinducible CO-Releasing Molecules, Eur. J. Inorg. Chem. 2011 (2011) 4571–4577.
[21] P. Govender, S. Pai, U. Schatzschneider, G.S. Smith, Next generation photocorms: polynuclear tricarbonylmanganese(I)-functionalized polypyridyl metallodendrimers, Inorg. Chem. 52 (2013) 5470–5478.
[22] A.C. Kautz, P.C. Kunz, C. Janiak, CO-releasing molecule (CORM) conjugate systems, Dalton Trans. 45 (2016) 18045–18063.
[23] R. Motterlini, B.E. Mann, R. Foresti, Therapeutic applications of carbon monoxide-releasing molecules, Expert Opin. Inv. Drugs 14 (2005) 1305–1318.
[24] S.J. Carrington, I. Chakraborty, P.K. Mascharak, Exceptionally rapid CO release from a manganese(I) tricarbonyl complex derived from bis(4-chloro-phenylimino) acenaphthene upon exposure to visible light, Dalton Trans. 44 (2015) 13828–13834.
[25] J. Meng, Z. Jin, P. Zhao, B. Zhao, M. Fan, Q. He, A multistage assembly/disassembly strategy for tumor-targeted CO delivery, Sci. Adv. 6 (2020) eaba1362.
[26] Y. Naito, K. Uchiyama, T. Takagi, T. Yoshikawa, Therapeutic potential of carbon monoxide (CO) for intestinal inflammation, Curr. Med. Chem. 19 (2012) 70–76.
[27] Q. Chen, Y. Yang, X. Lin, W. Ma, G. Chen, W. Li, X. Wang, Z. Yu, Platinum(iv) prodrugs with long lipid chains for drug delivery and overcoming cisplatin resistance, Chem. Comm. 54 (2018) 5369–5372.
[28] Y. Yu, Q. Xu, S. He, H. Xiong, Q. Zhang, W. Xu, V. Ricotta, L. Bai, Q. Zhang, Z. Yu, J. Ding, H. Xiao, D. Zhou, Recent advances in delivery of photosensitive metal-based drugs, Coord. Chem. Rev. 387 (2019) 154–179.
[29] H. Inaba, K. Fujita, T. Ueno, Design of biomaterials for intracellular delivery of carbon monoxide, Biomater. Sci. 3 (2015) 1423–1438.
[30] H.P. Joshi, S.B. Kim, S. Kim, H. Kumar, M.J. Jo, H. Choi, J. Kim, J.W. Kyung, S. Sohn, K.T. Kim, J.K. Kim, I.B. Han, Nanocarrier-mediated Delivery of CORM-2 Enhances Anti-allodynic and Anti-hyperalgesic Effects of CORM-2, Mol. Neurobiol. 56 (2019) 5539–5554.
[31] W. Adach, B. Olas, A comparison of the effects of the lipid-soluble CORM-2 and the water-soluble CORM-3 and CORM-A1 on platelet adhesion: The role of arachidonic acid metabolism, Thromb. Res. 188 (2020) 61–64.
[32] Z. Jin, Y. Wen, L. Xiong, T. Yang, P. Zhao, L. Tan, T. Wang, Z. Qian, B.-L. Su, Q. He, Intratumoral H2O2-triggered release of CO from a metal carbonyl-based nanomedicine for efficient CO therapy, ChemComm. 53 (2017) 5557–5560.
[33] Q. He, D.O. Kiesewetter, Y. Qu, X. Fu, J. Fan, P. Huang, Y. Liu, G. Zhu, Y. Liu, Z. Qian, X. Chen, NIR-Responsive On-Demand Release of CO from Metal Carbonyl-Caged Graphene Oxide Nanomedicine, Adv. Func. Mater. 27 (2015) 6741–6746.
[34] C. Bischof, T. Joshi, A. Dimri, L. Spiccia, U. Schatzschneider, Synthesis, spectroscopic properties, and photoinduced CO-release studies of functionalized ruthenium(II) polypyridyl complexes: versatile building blocks for development of CORM-peptide nucleic acid bioconjugates, Inorg. Chem. 52 (2013) 9297–9308.
[35] B.W. Sun, Y. Sun, Z.W. Sun, X. Chen, CO liberated from CORM-2 modulates the inflammatory response in the liver of thermally injured mice, World J. Gastroenterol. 14 (2008) 547–553.
[36] M.N. Pinto, P.K. Mascharak, Light-assisted and remote delivery of carbon monoxide to malignant cells and tissues: Photochemotherapy in the spotlight, J. Photochem. Photobiol., C 42 (2020), 100341.
[37] R. Sakla, D.A. Jose, Vesicles Functionalized with a CO-Releasing Molecule for Light-Induced CO Delivery, ACS Appl. Mater. Interfaces 10 (2018) 14214–14220.
[38] D. Wu, X. Duan, Q. Guan, J. Liu, X. Yang, F. Zhang, P. Huang, J. Shen, X. Shuai, Z. Cao, Mesoporous Polydopamine Carrying Manganese Carbonyl Responds to Tumor Microenvironment for Multimodal Imaging-Guided Cancer Therapy, Adv. Funct. Mater. 29 (2019) 1900095.
[39] Y. Li, J. Dang, Q. Liang, L. Yin, Carbon monoxide (CO)-Strengthened cooperative bioreductive anti-tumor therapy via mitochondrial exhaustion and hypoxia induction, Biomaterials 209 (2019) 138–151.
[40] J. Yao, Y. Liu, J. Wang, Q. Jiang, D. She, H. Guo, N. Sun, Z. Pang, C. Deng, W. Yang, S. Shen, On-demand CO release for amplification of chemotherapy by MOF functionalized magnetic carbon nanoparticles with NIR irradiation, Biomaterials 195 (2019) 51–62.
[41] A. Loureiro, G.J. Bernardes, U. Shimanovich, M.P. Sarria, E. Nogueira, A. Preto, A. C. Gomes, A. Cavaco-Paulo, Folic acid-tagged protein nanoemulsions loaded with CORM-2 enhance the survival of mice bearing subcutaneous A20 lymphoma tumors, Nanomedicine 11 (2015) 1077–1083.
[42] A. López de Guereñu, P. Bastian, P. Wessig, L. John, M.U. Kumke, Energy Transfer between Tm-Doped Upconverting Nanoparticles and a Small Organic Dye with Large Stokes Shift, Biosensors (Basel) 9 (2019) 9.
[43] M. Guan, H. Dong, J. Ge, D. Chen, L. Sun, S. Li, C. Wang, C. Yan, P. Wang, C. Shu, Multifunctional upconversion–nanoparticles–trismethylpyridylporphyrin–fullerene nanocomposite: a near-infrared light-triggered theranostic platform for imaging-guided photodynamic therapy, NPG Asia Mater. 7 (2015), e205.
[44] H.J. Kim, Y. Joe, J.S. Kong, S.-O. Jeong, G.J. Cho, S.W. Ryter, H.T. Chung, Carbon monoxide protects against hepatic ischemia/reperfusion injury via ROS-dependent Akt signaling and inhibition of glycogen synthase kinase 3β, Oxid. Med. Cell. Longev. 2013 (2013) 306421.
[45] B. Das, S. Lohar, A. Patra, E. Ahmmed, S.K. Mandal, J.N. Bhakta, K. Dhara, P. Chattopadhyay, A naphthalimide-based fluorescence "turn-on'' chemosensor for

highly selective detection of carbon monoxide: imaging applications in living cells, New J. Chem. 42 (2018) 13497–13502.
[46] M. Klinger-Strobel, S. Gläser, O. Makarewicz, R. Wyrwa, J. Weisser, M.W. Pletz, A. Schiller, Bactericidal Effect of a Photoresponsive Carbon Monoxide-Releasing Nonwoven against Staphylococcus aureus Biofilms, Antimicrob. Agents Chemother. 60 (2016) 4037–4046.
[47] A. Gabizon, A.T. Horowitz, D. Goren, D. Tzemach, F. Mandelbaum-Shavit, M. M. Qazen, S. Zalipsky, Targeting folate receptor with folate linked to extremities of poly(ethylene glycol)-grafted liposomes, in vitro studies, Bioconjugate Chem. 10 (1999) 289–298.
[48] Z.C. Soe, B.K. Poudel, H.T. Nguyen, R.K. Thapa, W. Ou, M. Gautam, K. Poudel, S. G. Jin, J.-H. Jeong, S.K. Ku, H.-G. Choi, C.S. Yong, J.O. Kim, Folate-targeted nanostructured chitosan/chondroitin sulfate complex carriers for enhanced delivery of bortezomib to colorectal cancer cells, Asian J. Pharm. 14 (2019) 40–51.
[49] V.M. Le, T.D.T. Nho, H.T. Ly, T.S. Vo, H.D. Nguyen, T.T.H. Phung, A. Zou, J. Liu, Enhanced anticancer efficacy and tumor targeting through folate-PEG modified nanoliposome loaded with 5-fluorouracil, Adv. Nat. Sci.: Nanosci. Nanotechnol. 8 (2017), 015008.
[50] A.E. Guller, A.N. Generalova, E.V. Petersen, A.V. Nechaev, I.A. Trusova, N. N. Landyshev, A. Nadort, E.A. Grebenik, S.M. Deyev, A.B. Shekhter, A.V. Zvyagin, Cytotoxicity and non-specific cellular uptake of bare and surface-modified upconversion nanoparticles in human skin cells, Nano Res. 8 (2015) 1546–1562.
[51] H.Q. Doan, K.A. Bowen, L.A. Jackson, B.M. Evers, Toll-like receptor 4 activation increases Akt phosphorylation in colon cancer cells, Anticancer Res. 29 (2009) 2473–2478.
[52] B. Kalyanaraman, V. Darley-Usmar, K.J.A. Davies, P.A. Dennery, H.J. Forman, M. B. Grisham, G.E. Mann, K. Moore, L.J. Roberts 2nd, H. Ischiropoulos, Measuring reactive oxygen and nitrogen species with fluorescent probes: challenges and limitations, Free Radic. Biol. Med. 52 (2012) 1–6.

Supporting Information

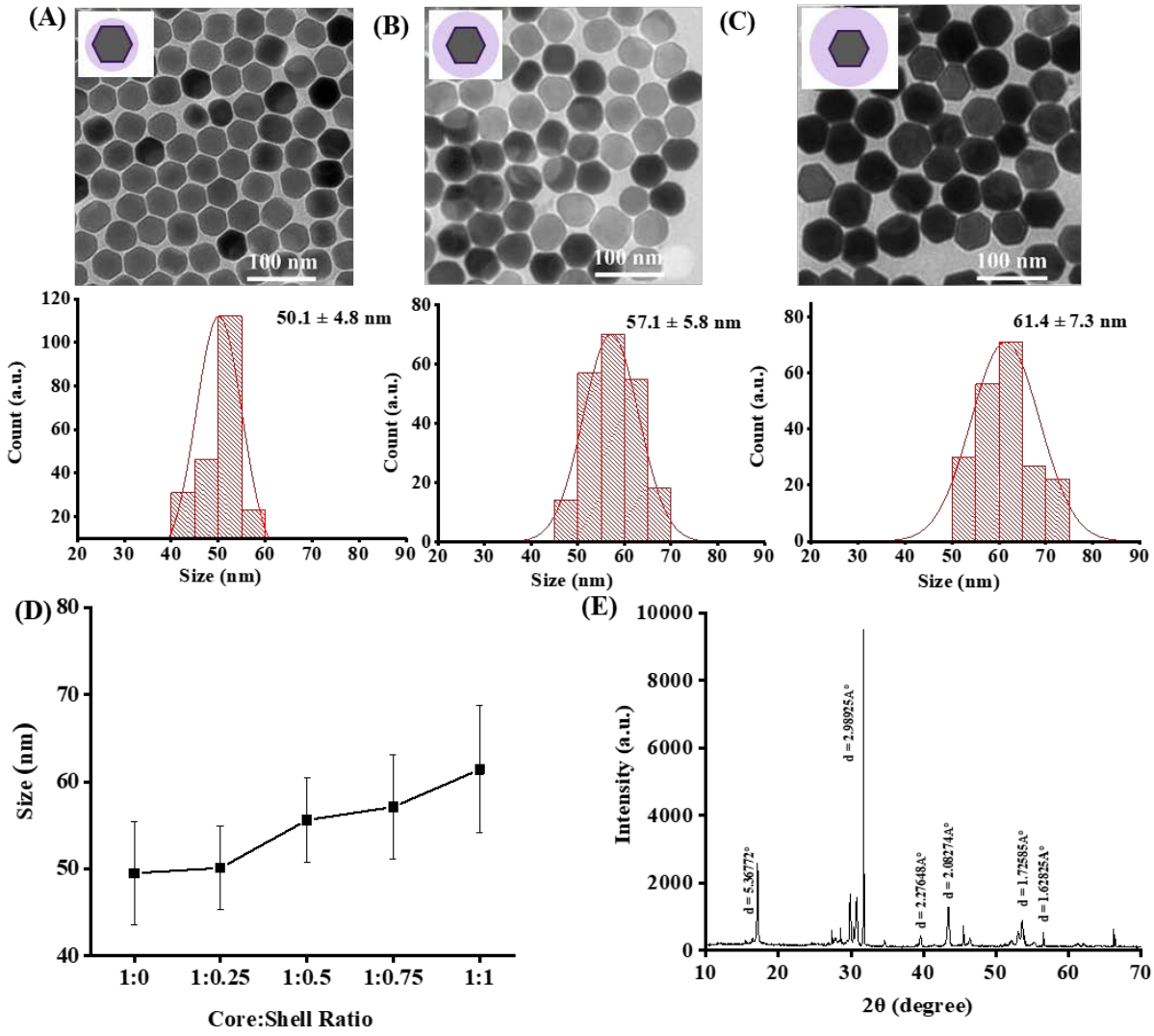

Figure S1. TEM imaging showing the morphology and particle size distribution of core-shell $NaYF_4$: Yb, Tm@ $NaYF_4$: Nd (1:0.25), core- shell $NaYF_4$: Yb, Tm@ $NaYF_4$: Nd (1:0.75) and core- shell $NaYF_4$: Yb, Tm@ $NaYF_4$: Nd nanoparticles (1:1) (A-C) (D) Variations in core-shell sizes for different ratios (E) X-ray diffraction spectra of core-shell nanoparticles

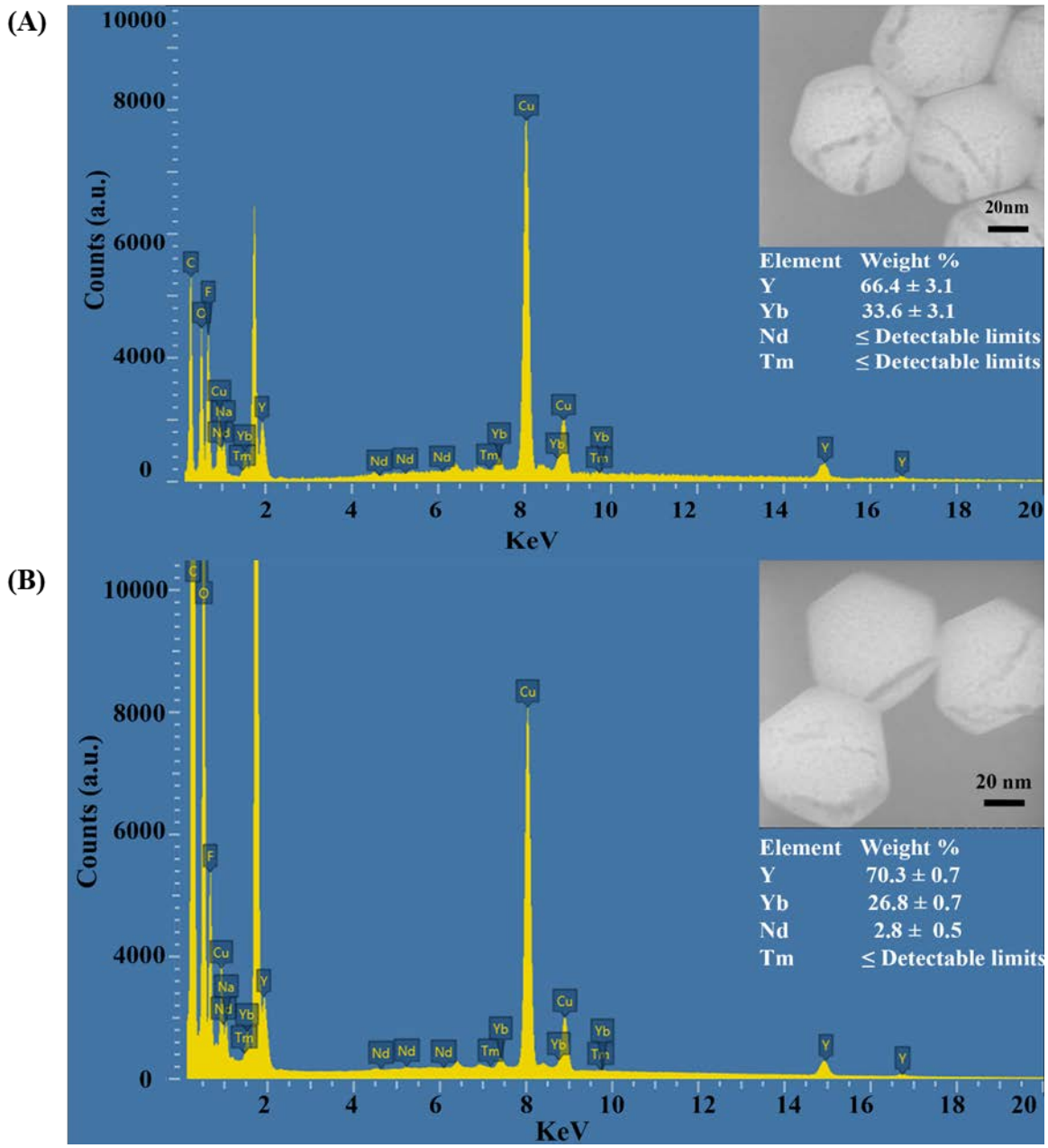

Figure S2. (A) STEM image and EDS analysis of lanthanides present in Core-Shells (1:0.5 ratio) (B) STEM image and EDS analysis of lanthanides present in Core-Shells (1:1 ratio)

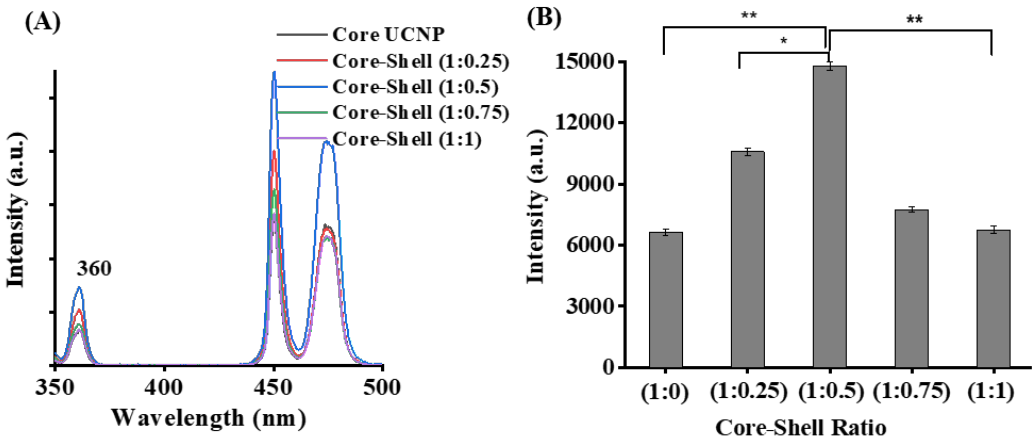

Figure S3. (A) Photoluminescence spectra of core $NaYF_4$: Yb, Tm and $NaYF_4$: Yb, Tm@ $NaYF_4$: Nd core-shell nanoparticles with different ratios at 980 nm (B) Comparison of different core-shell ratios and their 360 nm PL intensity

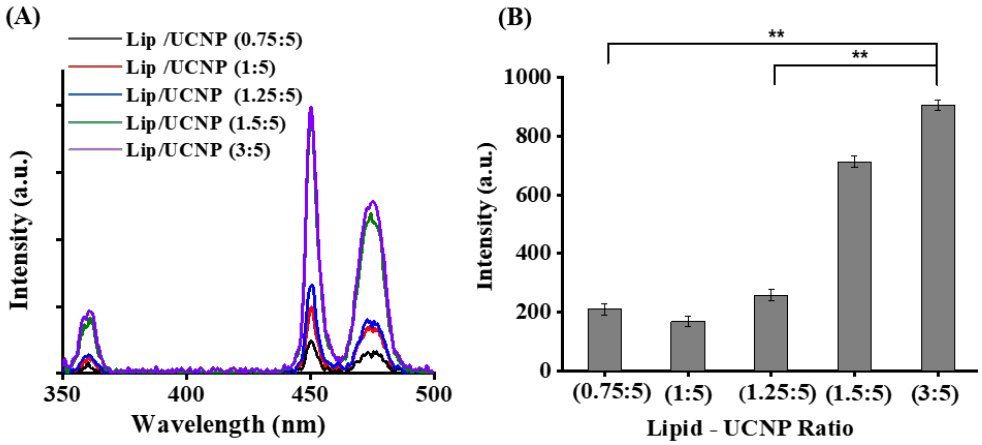

Figure S4. (A) Photoluminescence spectra of core $NaYF_4$: Yb, Tm and $NaYF_4$: Yb, Tm@ $NaYF_4$: Nd core-shell nanoparticles with different ratios at 980 nm (B) Comparison of different core-shell ratios and their 360 nm PL intensity

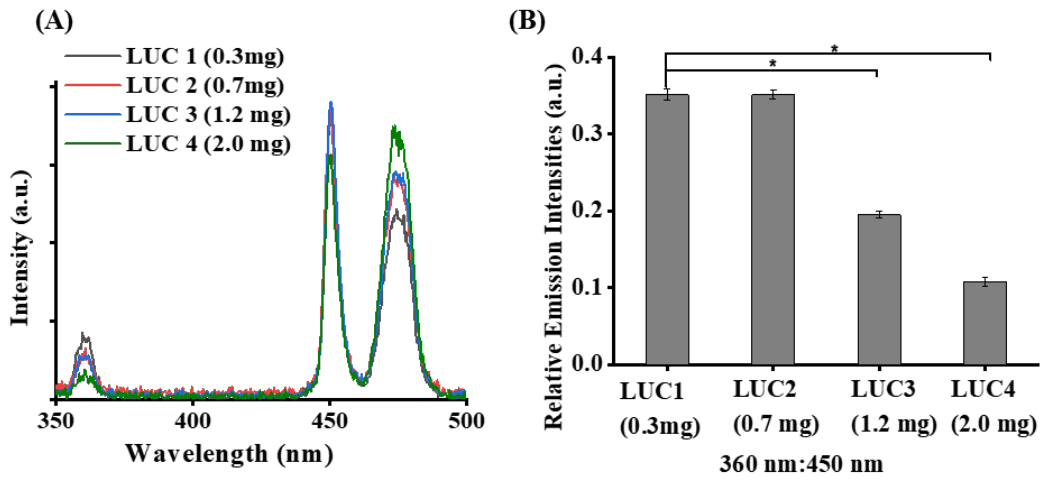

Figure S5. (A) PL Spectra for Optimization of final LUC nanoparticles with different amounts of drugs. (B) Relative intensities of PL spectra for different mixtures indicating the intensity at 360 nm compared to 475 nm.

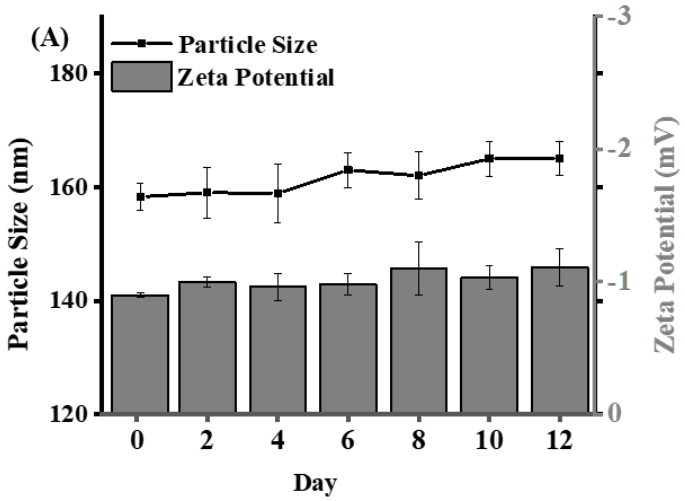

Figure S6 Particle size and Zeta Potential variation of final LUCF nanoparticles after 12 days of storage at 4 ºC.

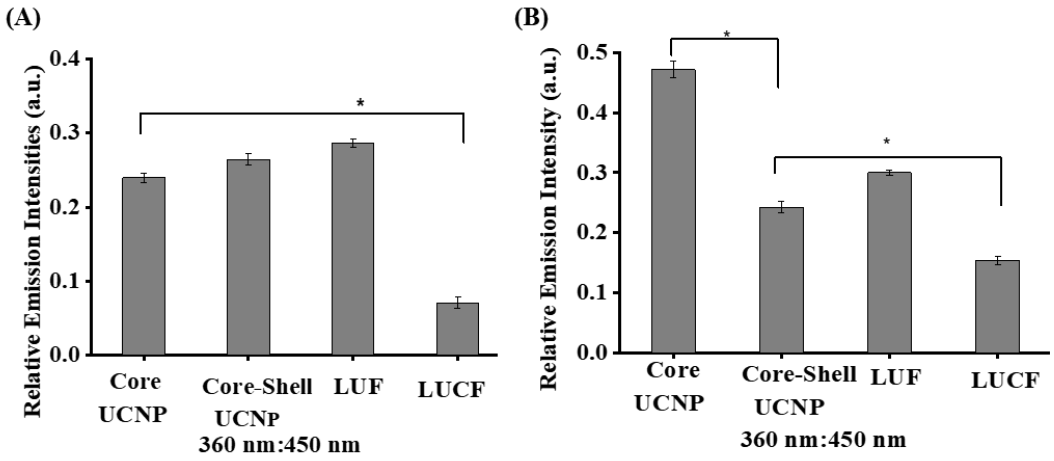

Figure S7. Ratio of highest peak to lower peak at different stages of drug formulation indicating the overlapping of CO absorbance at 360 nm for (A) 980 nm PL luminescence. (B) 808 nm PL luminescence.

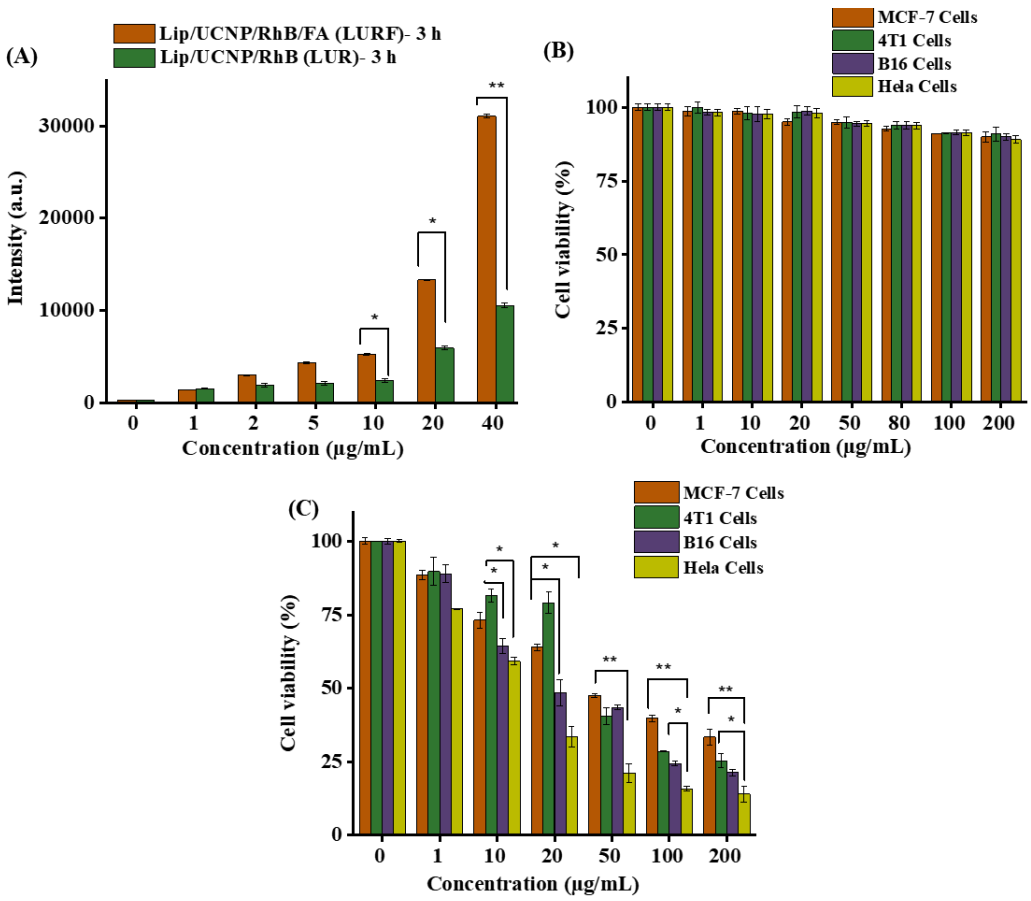

Figure S8 (A) Cell uptake for LUR and LURF nanoparticle with different concentrations of nanoparticles within 3 h (B) Cell viability assay of lipid-coated UCNPs (LUF) in different FA positive cell lines with 808 nm NIR light irradiation at 1 W/cm^2 and incubated without nanoparticle washing for 48 h. (C) Cell viability assay of lipid-coated UCNPs and CORM (LUCF) in different FA positive cell lines with 808 nm NIR light irradiation at 1 W/cm^2 for 5 min and incubated without nanoparticle washing for 48 h. Data are expressed as mean ± SD, *n* = 5, (*p < 0.05, **p < 0.01)

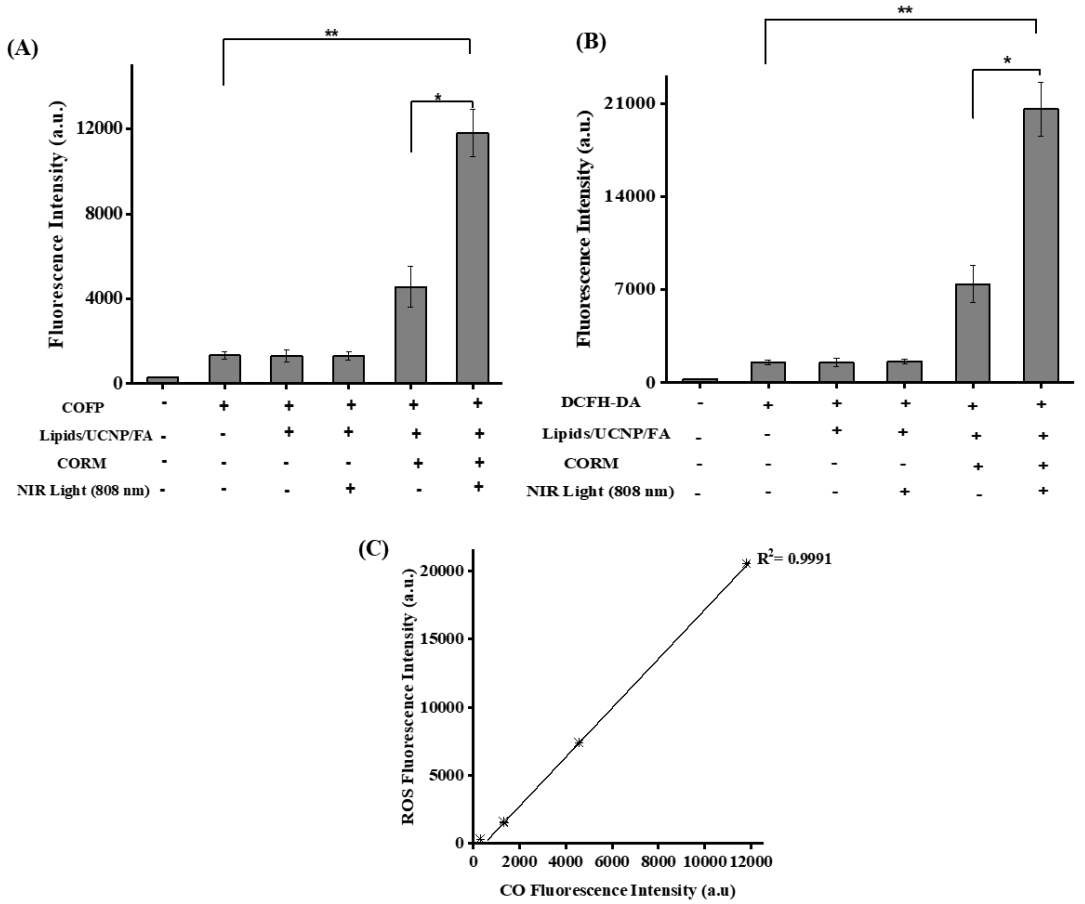

Figure S9. (A) Fluorescent intensity measurement of COFP signals in cells using a plate reader (λ_{ex}= 440 nm and λ_{em}= 520 nm) and mean fluorescence intensity from flow cytometry analysis of intracellular CO release in HCT116 cells after treatment with nanoparticles. (B) Fluorescent intensity measurement of ROS signals in cells using a plate reader (λ_{ex}= 495 nm and λ_{em}= 525 nm) and mean fluorescence intensity from flow cytometry analysis of intracellular ROS release in HCT116 cells after treatment with nanoparticles. (C) Graph of intracellular CO fluorescent measurement with respect to ROS generated after cell treatment.

Table S1: Optimization of lipids and UCNP drug delivery system

Name	Composition/ (DOPC: DOPA: Cholesterol: DSPE-PEG:DSPE-PEG-FA) ratio	Hydrodynamic diameter (nm)	Zeta potential (mV)	Polydispersity index (PDI)
Lip/UCNP/ FA(LUF1)	0.75 mg (45:35:10:5:5)	154.9 ± 3.8	0.2 ± 0.1	0.23 ± 0.04
Lip/UCNP/ FA (LUF2)	1.0 mg (45:35:10:5:5)	152.8 ± 4.9	-0.1 ± 0.1	0.24 ± 0.06
Lip/UCNP/ FA (LUF3)	1.25 mg (45:35:10:5:5)	152.8 ± 4.6	-1.4 ± 0.8	0.25 ± 0.05
Lip/UCNP/ FA (LUF4)	1.5 mg (45:35:10:5:5)	153.9 ± 2.8	-3.1 ± 2.0	0.21 ± 0.02
Lip/UCNP/ FA (LUF5)	3.0 mg (45:35:10:5:5)	160.5 ± 3.5	-6.9± 2.9	0.26 ± 0.13
Lip/UCNP/ FA (LUF6)	1.5 mg (40:40:10:5:5)	158.4 ± 2.1	-5.1 ± 2.9	0.25 ± 0.15

Table showing the characteristic properties of formulated nanoparticles (LUF) with 5 mg UCNPs during the optimization process

Table S2: Optimization of lipids, UCNP and CORM

Name	Lipid: UCNP:CORM ratio	DOPC: DOPA: Cholesterol: DSPE-PEG: DSPE-PEG-FA ratio	Hydrodynamic diameter (nm)	Zeta potential (mV)	Drug Loading (%)
Lip/UCNP/CORM/FA (LUCF1)	**(2:5:0.3)**	**(45:35:10:5:5)**	154.3± 2.8	-1.0 ± 0.4	2.52
Lip/UCNP/CORM/FA (LUCF2)	**(2:5:0.7)**	**(45:35:10:5:5)**	159.8 ± 4.9	-0.2 ± 0.1	4.69
Lip/UCNP/CORM/FA (LUCF3)	**(2:5:1.2)**	**(45:35:10:5:5)**	158.5 ± 2.4	6.4 ± 0.9	7.90
Lip/UCNP/CORM/FA (LUCF4)	**(1.5:5:2.0)**	**(45:35:10:5:5)**	162.5 ± 2.6	12.2 ± 0.7	19.01
Lip/UCNP/CORM/FA (LUCF5)	**(1.5:5:2.0)**	**(40:40::10:5:5)**	158.3 ± 3.9	-0.9 ± 0.2	18.10

Table showing the characteristic properties of CORM delivery system with variable amounts of CORM and the optimized amount of lipids and UCNPs.

Table S3: Optimization of lipids, UCNP and Rhodamine-B.

Name	Rhodamine-B Composition (µg)	Hydrodynamic diameter (nm)	Zeta potential (mV)
Lip/UCNP/ Rhodamine-B (LUR)	30	145.2 ± 1.2	-1.3 ± 0.2
Lip/UCNP/Rhodamine –B /FA (LURF)	30	146.9 ± 0.9	-1.2 ± 0.3

Table showing the characteristic properties of rhodamine-B encapsulated delivery system with or without folates.